NATIONAL HIGH MAGNETIC FIELD LABORATORY

MAG LAB REPORTS

HIGHLIGHTS FROM THE 2008 ANNUAL REPORT

FSU • UF • LANL

TABLE OF CONTENTS

CONDENSED MATTER PHYSICS

Kondo/heavy fermion systems; magnetism and magnetic materials; metal-insulator transitions; molecular conductors; other condensed matter; quantum fluids and solids; semiconductors; quantum fluids and solids; semiconductors; superconductivity-basic

DIRECTOR'S INTRODUCTION

Welcome to the 2008 Highlights Issue

Well, we kept all the magnets running in 2008, despite some real budget crunches. And as a result 2008 featured some spectacular science, highlights of which are included in this issue.

First, a few words about research reports: At the end of each year, we ask our users and research faculty at The Florida State University, University of Florida and Los Alamos National Lab to submit one-page abstracts of their MagLab research endeavors. The deal is this: users get the magnet time and all that comes with it (instrumentation, cryogens, scientific and technical expertise of MagLab scientists, etc) and we get a short one-page summary of the research performed. Not a bad deal.

We don't just file the reports away. Although they fulfill our contractual obligation to the National Science Foundation (and ultimately the taxpayers!) under the National Science Foundation's Government Performance and Results Act, we also find them extremely useful, as they provide a snapshot of research underway or recently completed.

Research reports are a different measure of activity than publications in refereed journals. They summarize level of activity – and direction – of scientific inquiry at the lab, rather than just presenting the published successes. To be sure, they are in many ways a leading indicator of scientific publications:

➤ 21% of the research activities (80 reports) were already published in 2008, many in prominent journals including *Nature, Nature Physics, Science, Physical Review Letters, Analytical Chemistry, IEEE Transactions on Applied Superconductivity, Journal of the American Chemical Society* and *Proceedings of the National Academy of Science.*

➤ Another 8% of the reports were accepted for publication; 10% were submitted for publication; and 36% have manuscripts in preparation.

What goes into this Highlights Issue? After we receive all of the research reports from our users and facility directors/department heads approve them, the Magnet Lab Science Council reviews the reports. The Science Council, composed of leading research scientists representing all three Magnet Lab sites, helps me understand the lab's scientific activity. Among other things, it makes my job a whole lot easier by going through each report and recommending a few dozen for consideration as highlights. The Science Council is: Albert Migliori, LANL fellow, Pulsed Field Facility (chairman); Rafael Brüschweiler, associate director for Biophysics, NMR; Mark Emmett, scholar-scientist, ICR; Lev Gor'kov, program director, professor, Condensed Matter Science/Theory; Stephen Hill, director, EMR Program; David Larbalestier, director, Applied Superconductivity Center; Denis Markiewicz, engineer, Magnet Science & Technology; Dragana Popovic, scholar-scientist, Condensed Matter/Experimental; and Glenn Walter, associate professor, AMRIS.

The criteria for selection of a given report as a highlight emphasizes research that is published, features a new technique for future users, and showcases outstanding research. Together, the highlights span all three Magnet Lab sites and seven user programs. As such, the highlights represent the Magnet Lab's broad research portfolio in a concise format for a scientific, non-specialist audience.

Of the 377 research reports submitted in 2008, the Science Council recommended 56: 14 in life sciences, 11 in chemistry, 8 in magnet science and technology, and 23 in condensed matter physics. I further whittled them down to 33.

Why 33 Highlights this year? It's not just because it's not a prime number. These highlights represent real innovation and breakthroughs, many of which relied specifically on the uniqueness of our magnets and experimental capabilities. That tends to push the number of highlights higher each year, but we try to keep the number down to do some justice to the word "highlight."

One of the biggest highlights this year? The new pnictide superconductors. Much to the scientific community's delight, this material has a very large upper critical field. Both the DC and Pulsed Field user programs were inundated with – and accommodated – requests for the study of these remarkable compounds, hosting several different and competing groups simultaneously throughout much of the summer (pages 46-49).

MagLab-engineered techniques and state-of-the-art probes continue to serve user research in condensed matter physics…

➤ Heat capacity and magnetocaloric effect experiments in the hybrid and pulsed magnets that reveal a third distinct ordered state for the spin-one triangular lattice in $Ba_3Mn_2O_8$ (page 31);
➤ High-magnetic-field optical spectroscopy, magnetization and other techniques to study electronically driven multiferroicity in $LuFe_2O_4$ that demonstrates the important interplay among charge, structure and magnetism (page 30);
➤ First observation of spin echoes from high-spin, single-molecule magnet single crystals – made possible through the MagLab's custom high-frequency electron magnetic resonance instrumentation (page 40); and
➤ Research at an unmatched ratio of B/T (B~16T and T~1mK) to study field-induced Bose-Einstein condensation in an organic compound by demonstrating the 3/2 power-law exponent in the temperature dependence of the critical field line (page 41).

…as well as user research from materials research and solid-state chemistry to organic chemistry and biomedicine, using a wide array of both electron and nuclear magnetic resonance techniques:

➤ Detecting quadrupolar nuclei using the very narrow bore 830 MHz spectrometer and unique high sensitivity probes (page 18);
➤ 750 MHz Magic Angle Spinning probe that defines the cutting-edge for both signal-to-noise radio and heating (page 21); and
➤ Low-electric field NMR probes to minimize sample heating from RF irradiation, used in the 900 MHz magnet as well as the lab's 600 and 400 MHz magnets (page 7).

…as well as user research that expands the MagLab's leading Fourier transform ion cyclotron resonance (FT-ICR) program:

➤ Pioneering the field of petroleomics, to compile the complete listing of molecular constituents in a given sample of petroleum: a chemical 'fingerprint' that enables a wide range of new energy-related research, much as genomics did for biomedical research (page 14).

On the magnet science and technology front, work on cable in conduit conductors will benefit the MagLab's new Series Connected Hybrid user magnet under development for a 2012 delivery. It also greatly assisted the international magnet community and in particular, the Department of Energy's ITER project, the international research and development project that aims to demonstrate the scientific and technical feasibility of fusion power (pages 22, 23).

And, oh yeah, the upcoming revolution in superconducting magnets. Thirty-four – count 'em, 34 – teslas. Work this past year has provided a proof-of-principle that new high-temperature superconducting (YBCO) tape can be wound into an all-superconducting magnet that could exceed 30 teslas. This is a spectacular demonstration of new MagLab magnet technology, one that may free superconducting magnets from the "niobium-jailhouse" that limits their present performance to around 20 teslas (page 26).

Also notable in 2008:

➤ The User Collaboration Grants Program supported 39 of the 377 research activities and was the primary support for 11 projects. The program encourages collaborations among internal and external investigators and promotes risky but worthwhile attempts to push experimental techniques.
➤ The National Science Foundation, the Department of Energy and the National Institutes of Health funded the majority of research projects. Other U.S. funding organizations included: Human Frontiers Science Program, Muscular Dystrophy Association, NASA, U.S. Air Force Office of Scientific Research and the U.S. Environmental Protection Agency.
➤ Funding support for research also originated from around the world: the Deutsche Forschungsgemeinschaft (Germany), Engineering and Physical Sciences Research Council (UK), Japan Society for the Promotion of Science, National Sciences and Engineering Research Council (Canada), and the Russian Academy of Science.

Thanks go to the users, who give us excellent source materials to make an interesting issue. And special thanks to the Science Council and to Kathy Hedick, for guiding/gently prodding us through the process.

Rock and roll,

Gregory S. Boebinger

GREGORY S. BOEBINGER

DIRECTOR'S INTRODUCTION

LIFE SCIENCES

Researchers using the high-sensitivity 1-mm HTS probe in AMRIS were able to connect mating behavior with dauer formation in C. elegans for the first time. These findings have important implications related to controlling parasitic infestations.

• This research was published in *Nature*, **454**, 1115-1118 (2008).

Identification of the *Caenorhabditis elegans* Mating Pheromone

J. Srinivasan (Caltech, Biology); F. Kaplan (UF, Biochem); R. Ajredini (UF, Biochem); C. Zachariah (UF, Biochem); H.T. Alborn (USDA Labs, Gainesville); P.E.A. Teal (USDA Labs, Gainesville); R.U. Malik (Cornell, Chemistry); A.S. Edison (UF, Biochem); P.W. Sternberg (Caltech/HHMI, Biology); F.C. Schroeder (Cornell, Chemistry)

INTRODUCTION

C. elegans is a free-living soil-dwelling nematode that develops through four larval stages to 1-mm long adults in about 3.5 days. If food is scarce, *C. elegans* enters a developmentally arrested stage called dauer that allows animals to survive for extended periods with no food. Male *C. elegans* are chemically attracted to hermaphrodites, and we used NMR, mass spectrometry and activity-guided fractionation to show that a group of molecules called ascarosides controls both mating and dauer. At low concentrations, a synergistic mix causes male attraction and at higher concentrations, the same molecules induce dauer formation.

EXPERIMENTAL, RESULTS AND DISCUSSION

Worms were grown to defined developmental stages, transferred to water and incubated for one hour to collect secreted molecules. We then assayed the worm-conditioned water (WW) to test for its ability to specifically attract male *C. elegans*. We found that WW from developmental stages in which worms become fertile attracted males. We then separated active material by hydrophobicity followed by charge and assayed each fraction for activity. We found that three closely related molecules act together synergistically at picomolar concentrations to attract males. At intermediate concentrations, the same compounds repel hermaphrodites, and at high nanomolar or micromolar concentrations, the compounds induce dauer formation[2].

CONCLUSIONS

This was the first study to connect mating behavior with dauer formation in *C. elegans*. The dose-dependent and synergistic responses of the compounds raise many possibilities for additional chemical signaling and also suggest novel ways for controlling parasitic crop or animal nematodes in the future.
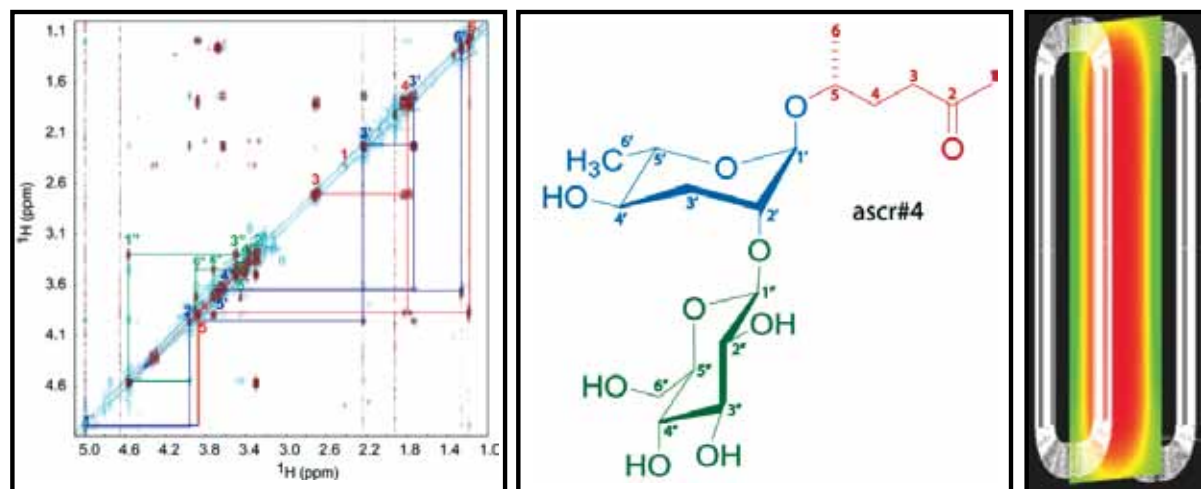

Figure 1.
The Magnet Lab 1-mm HTS probe (right schematic) was critical for this study[1]. We used about 0.4 L of culture to obtain the material for the COSY and NOESY spectra (left) of one of the pheromones (middle). Previous studies utilized over 300 L to identify the first dauer pheromone.

LIFE SCIENCES

REFERENCES
1. W. Brey *et al.*, *J Magn Reson*, **179**, 290-293 (2006).
2. J. Srinivasan *et al.*, *Nature*, **454**, 1115-1118 (2008).

Phospholamban is an essential integral membrane protein in heart cells. Using Magnet Lab hardware and methodology including 600 MHz low-E probe and Polarization Inversion Spin Exchange at Magic Angle (PIESMA) pulse sequence, the structure and topology of this protein in DOPC lipid bilayers was determined.

• This work has been accepted by the *Journal of Biomolecular NMR* and a second manuscript is under review.

Topology and Structure of Phospholamban Monomer in Oriented DOPC Lipid Bilayers

N.J. Traaseth, R. Verardi, L. Shi, G. Veglia (U. of Minnesota, Dept. of Biochemistry, Molecular Biology and Biophysics)

INTRODUCTION

Phospholamban (PLN) is an essential integral membrane protein within the sarcoplasmic reticulum (SR) of cardiac myocytes. Within the membrane, PLN is an endogenous inhibitor of SR Ca-ATPase (SERCA) that is believed to be important in two oligomeric forms: a) a monomer that directly binds to and inhibits SERCA[1] and b) a pentamer that acts as a storage form within the SR membrane[1]. In this work, we looked at the structure and topology of PLN monomer in mechanically oriented lipid bilayers using the solid-state NMR experiment PISEMA.
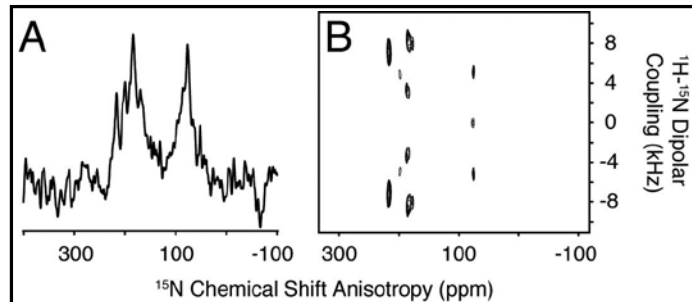
Figure 1.
A. 1D cross-polarization spectrum of [15N-Leu] PLN in DOPC lipid bilayers.
B. PISEMA spectrum of the same sample in A.

Figure 2.
Structure and topology of monomeric PLN refined in explicit DOPC lipid bilayers that agrees with all solid-state and solution NMR restraints.
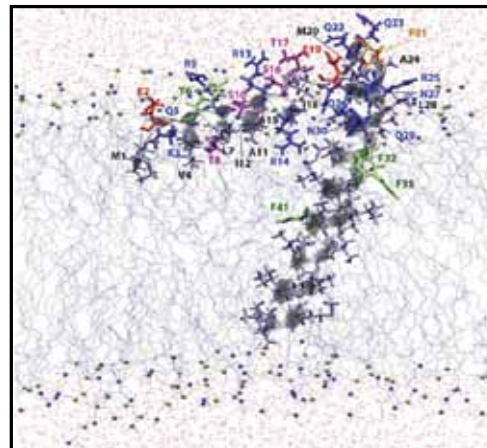
EXPERIMENTAL

A fully functional monomeric mutant of PLN (C36A, C41F, C46A) was selectively labeled with 15N-Leu and reconstituted into mechanically aligned lipid bilayers as previously described[2]. The final lipid/protein molar ratio was ~150/1. A 2D PISEMA experiment was acquired with 4k scans and 12 increments at 35° C with a recycle delay of 5 sec. The spectrum was acquired at a 14.1 tesla field strength (1H frequency of 600.1 MHz) equipped with a Bruker DMX spectrometer at the Magnet Lab in Tallahassee using a low-E probe with a doubly tuned, low-inductance resonator built by the Magnet Lab's RF program[3].

RESULTS AND DISCUSSION

Figure 1 shows the results from the 1D cross-polarization and PISEMA experiments acquired using a selectively labeled 15N-Leu PLN. Since 9 of the 10 leucine residues are within the transmembrane portion of the spectrum, the majority of the signals resonate in the downfield portion of the spectrum (~200 ppm), indicating good alignment. Using the results from this spectrum and other selectively labeled samples, we were able to determine the 24° tilt angle that the membrane embedded helical domain makes with respect to the lipid bilayer normal[2, 4].

LIFE SCIENCES

CONCLUSIONS

We have used PISEMA solid-state NMR spectroscopy at the Magnet Lab to determine the structure and topology of monomeric PLN (Figure 2), which has recently been submitted for publication[4].

REFERENCES

1. Y. Kimura, *et al., J Biol Chem*, **272**, 15061-15064 (1997).
2. N.J. Traaseth *et al., Biochemistry*, **45**, 13827-13834 (2006).
3. P.L. Gor'kov *et al., J Magn Reson*, **185**, 77-93 (2007).
4. N.J. Traaseth *et al.,* Submitted.

This report describes a strategy for the semi-automated deconvolution of complex mixture spectra encountered in metabolomics, in the present case, a cancer cell extract. It demonstrates the utility of combining ^{13}C spectroscopy with ^{1}H spectroscopy to unambiguously identify the complex mixture components. Several manuscripts of this and related work have appeared in *Analytical Chemistry*, an American Chemical Society journal. This analysis tool is implemented on the Complex Mixture Analysis by NMR (COLMAR) Web server at the Mag Lab (http://spinportal.magnet.fsu.edu), which attracts many users from all over the world.

• This work was published in *Analytical Chemistry,* **80** (19) 7549–7553 (2008).

COLMAR Web Server Assisted Metabolic Mixture Analysis by Heteronuclear NMR

F. Zhang (Magnet Lab), L. Bruschweiler-Li, S.L. Robinette, R. Brüschweiler (FSU, Chemistry, Magnet Lab)

INTRODUCTION

Identification of individual chemical components of biological systems and monitoring of their changes in response to a multitude of factors such as genetics, age, pathology, development, environment, stress and treatment are key aspects of metabolomics and metabonomics. The comprehensive systems biological approach to the study of metabolic mixtures thereby promises a better understanding of complex biochemical processes in living systems.

Here we present a generalization of the recently introduced homonuclear TOCSY-based DemixC method[1] to heteronuclear 2D HSQC-TOCSY NMR spectroscopy. The approach takes advantage of the high resolution afforded along the ^{13}C dimension due to the narrow ^{13}C line widths for the identification of spin systems and compounds.[3] The method combines information from both 1D ^{13}C and ^{1}H traces by querying them against an NMR spectral database using our public COLMAR query Web server at http://spinportal.magnet.fsu.edu[2] (Figure 1).

COLMAR Metabolomics Web Portal for Complex Mixture Analysis by NMR (COLMAR)

Figure 1.
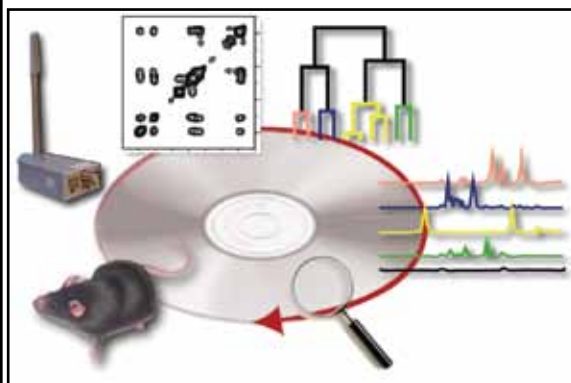Web portal at http://spinportal.magnet.fsu.edu/ consists of Covariance, DemixC, and Query Web servers.
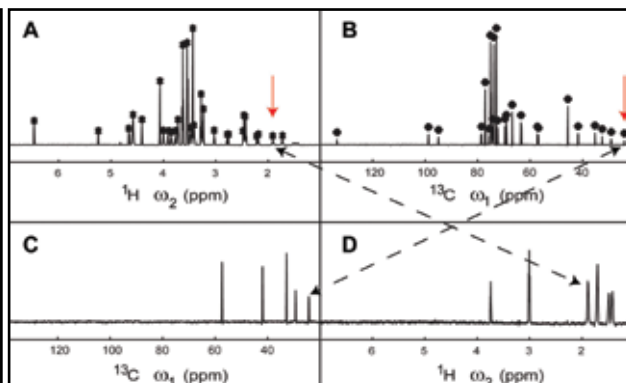
Figure 2.
Mixture analysis by heteronuclear NMR

LIFE SCIENCES

RESULTS AND DISCUSSION

Figure 2 shows the "importance index" profile determined from a 2D HSQC-TOCSY spectrum of a mixture consisting of five model compounds (A) along ^{1}H dimension and (B) along ^{13}C dimension. At the peak positions ("x" symbols) picked in panels A and B a subset of traces is extracted in the HSQC-TOCSY spectrum, such as the lysine carbon trace obtained from the ^{1}H importance index (panel C) and the lysine proton trace obtained from ^{13}C importance index (panel D). The vertical arrows indicate the importance index peak positions where the traces were extracted in the HSQC-TOCSY. The diagonal arrows indicate the connections between the importance index and the traces picked linking the ^{13}C (C) and ^{1}H (D) traces to the same compound (lysine)[3]. The complementarity of ^{13}C and ^{1}H spectral information thereby improves the robustness of compound identification, which has been demonstrated for a cancer cell extract.[3]

CONCLUSION

This type of metabolic mixture analysis by heteronuclear NMR is included in our COLMAR suite of Metabolomics Web portals. This and other COLMAR servers aid the semi-automated identification and quantification of chemical components of metabolomics mixtures without requiring physical separation of individual components. The Web portal, which is public, allows users easy uploading and downloading of data and thereby significantly facilitates the analysis of a wide range of complex biofluids by NMR spectroscopy.

ACKNOWLEDGEMENTS

REFERENCES

1. F. Zhang and R. Brüschweiler, *Angewandte Chemie Int. Ed.,* **46**, 2639 (2007); F. Zhang *et al.*, *Anal. Chem.*, **79**, 7748 (2007).
2. S. L. Robinette *et al.*, *Anal. Chem.*, **80**, 3606 (2008).
3. F. Zhang *et al.*, *Anal. Chem.*, **80**, 7549 (2008).

A new technique has been devised to perform electron magnetic resonance (EMR) studies on Vanadium(III) ion complexes in frozen buffer as opposed to conventional solid-state samples. This technique could prove to be instrumental in the EMR study of true biological samples.

• This work was published in the *Journal of Inorganic Biochemistry,* **103,** 487-495 (2009).
• This research was supported by the Magnet Lab User Collaboration Grants Program.

HFEPR Studies of Aminocarboxylate Complexes of Vanadium(III) in Frozen Aqueous Solution

J. Telser (Roosevelt U., Biological, Chemical and Physical Sciences); C.-C. Wu, K.-Y. Chen, H.-F. Hsu (National Cheng Kung U., Taiwan, Chemistry); A. Ozarowski, J. Krzystek (Magnet Lab, EMR)

INTRODUCTION

As an extension of investigating model complexes for the vanadium-containing nitrogenase enzyme (V-N$_2$ase),[1] we have pursued studies of complexes formed by the vanadium(III) ion (3d^2, $S = 1$) with ligands of biological relevance belonging to the well known class of aminocarboxylates.[2] The biological relevance of aminocarboxylate complexes of V(III) stems from two disparate areas: they are analogous to those in ascidian (sea squirt) blood cells,[3] and are also employed as insulin mimics.[4] Perfecting the methodology of recording HFEPR spectra in frozen solution was the focus of the current study, since such experimental conditions are more relevant to biological samples than are solid-state studies.

EXPERIMENTAL

The EMR facility with a 17 tesla (T) superconducting magnet was used in this specific
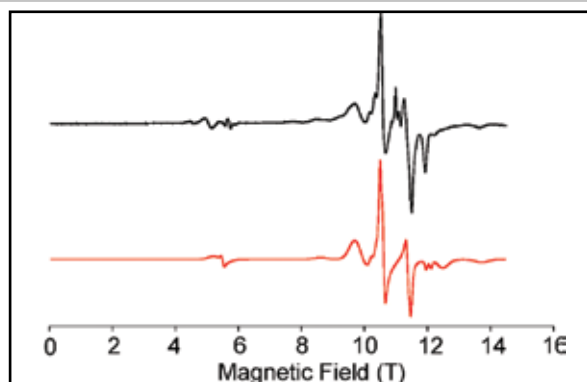
Figure 1.

HFEPR spectrum of aqueous [V(trdta)]$^-$ recorded at 305 GHz and 20 K (black trace) together with a simulation (red trace) assuming an ideal powder pattern, which is the sum of equal amounts of three individual triplet species. Spin Hamiltonian parameters used in the simulations: all $S = 1$; one species with $D = +0.68$ cm^{-1}, $E = 0$, $g_{x,y} = 1.98$, $g_z = 1.95$; one species with the same except, $D = +0.87$ cm^{-1}; one species with the same except: $D = +2.35$ cm^{-1}, $g_{iso} = 1.95$. The sharp peaks appearing near 11 T in the experimental trace are due to a minor V(IV) impurity.

LIFE SCIENCES

work. The solutions were prepared in degassed water with the pH adjusted to ~ 7. The V(III) concentrations were ~200 mM.

RESULTS AND DISCUSSION

All three of the investigated V(III) complexes (with nta, edta, and trdta ligands) gave HFEPR spectra in frozen aqueous solution at multiple frequencies and temperatures. A representative spectrum for the trdta complex is shown in Figure 1. As also indicated in the Figure 1 caption, full spin Hamiltonian parameters were extracted for multiple species of this complex, which can be related to possible isomerism in solution, resulting from aqua versus carboxylato ligand coordination.[2,3]

CONCLUSIONS

We have shown the ability of HFEPR to determine spin Hamiltonian parameters for the non-Kramers ion V(III) in frozen aqueous solutions. HFEPR is uniquely able to identify multiple species in solution, which optical measurements cannot distinguish. This demonstrates the potential of this technique for application to actual biological conditions.

Figure 2.
Molecular coordinate system defined for [V(trdta)]⁻.

ACKNOWLEDGEMENTS

REFERENCES
1. W.-C. Chu *et al.*, *Inorg. Chem.* **45**, 3164-3166 (2006).
2. K.-Y. Chen et al., NHMFL Research Report (2007); J. Telser *et al., J. Inorg. Biochem.,* **103**, 487-495 (2009).
3. K. Kanamori, *et al.*, *Inorg. Chem.*, **33**, 5547-5554 (1994).
4. V. Monga *et al.*, *Inorg. Chem.*, **44**, 2678-2688 (2005).

MLR

This report describes the characterization and use of a novel low pH active protease in Hydrogen/Deuterium Exchange (HDX) with high-resolution Fourier transform ion cyclotron resonance mass spectrometry MS (FT-ICR MS) analysis. Protease XIII provides enhanced amino acid sequence coverage, higher sensitivity and lower self digestion than the standard pepsin used in HDX experiments. Use of protease XIII in HDX experiments enables higher resolution protein conformational information to be acquired for understanding protein, protein/protein, and/or protein /ligand interaction. This methodology will benefit all laboratories that perform HDX experiments.

• This work was published in *Analytical Chemistry,* **80**, 9034-9041 (2008).

Enhanced Digestion Efficiency, Peptide Ionization Efficiency, and Sequence Resolution for Protein Hydrogen/Deuterium Exchange Monitored by FT-ICR Mass Spectrometry

H-M Zhang (FSU, Molecular Biophysics); S. Kazazic (Ruder Boskovic Inst.); T.M. Schaub (FSU, Magnet Lab); J.D.Tipton (FSU, Magnet Lab); M.R. Emmett (FSU, Magnet Lab); A.G. Marshall (FSU, Magnet Lab, Chemistry)

RESULTS AND DISCUSSION

Solution-phase hydrogen/deuterium exchange (HDX) monitored by high-resolution FT-ICR MS offers a rapid method to study protein conformations and protein-protein interactions. Pepsin is usually used to digest proteins in HDX and is known for lack of cleavage specificity. To improve digestion efficiency and specificity, we have optimized digestion conditions and cleavage preferences for pepsin and protease type XIII from *Aspergillus saitoi*. A dilution series of the proteases was used to determine the digestion efficiency for several test proteins. Protease type XIII prefers to cleave on the C-terminal end of basic amino acids
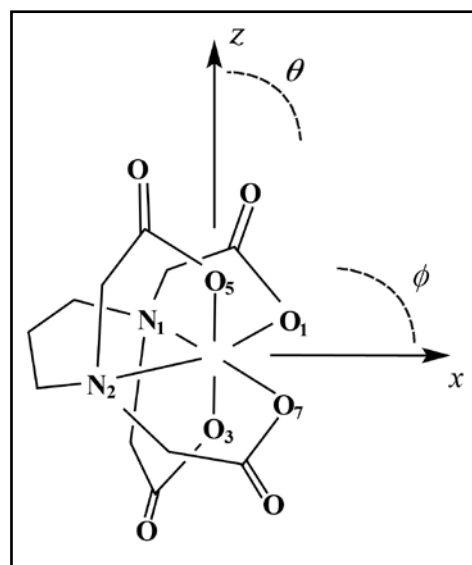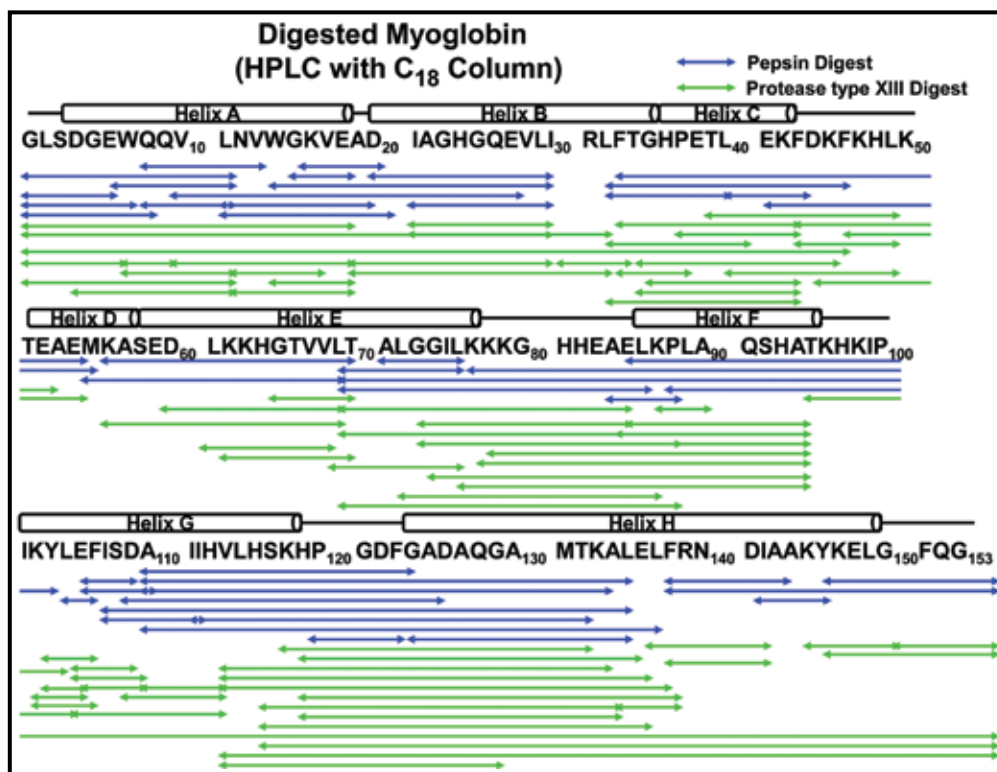
Figure 1.
A new enzyme "chews" myglobin (a test protein) into more "bite-sized" segments (**green**) than conventional treatment (**blue**). Subsequent separation and analysis of the fragments enables more complete and specific reconstruction of the exposed surfaces of the protein, making it possible to identify sites of binding of other agents (e.g., drugs or protein partners).

and produced the highest number of fragments and the best sequence coverage compared to pepsin or protease type XVIII from Rhizhopus (see Figure). Furthermore, protease type XIII exhibited much less self-digestion than pepsin and thus is superior for HDX experiments. Many highly overlapped segments from protease type XIII and pepsin digestion, combined with high-resolution FT-ICR mass spectrometry, provide high sequence resolution (to as few as one or two amino acids) for the assignment of amide hydrogen exchange rate. Our H/D exchange results correlate well with the secondary and tertiary structure of myoglobin. Such assignments of highly overlapped fragments promise to greatly enhance the accuracy and sequence resolution for determining conformational differences resulting from ligand binding or protein–protein interactions.

ACKNOWLEDGEMENTS

REFERENCES
1.   H.-M. Zhang *et al., Anal. Chem.*, **80**, 9034-9041 (2008).

LIFE SCIENCES

Functional magnetic resonance imaging (fMRI) is a commonly used tool to noninvasively visualize neuronal activation in both animals and humans. Despite a tremendously prolific field resulting in 19,000 publications since the 1992, only a small percentage (5%) of these publications have examined the true neurological basis of fMRI (see the editorial in *Nature Neuroscience* 12(2):2009,p99). With this lack of basic understanding of the mechanisms that results in fMRI signals, there is a great need to develop model systems that are capable of manipulating and imaging neuronal activity in a controlled manner. This may now be possible through the use of high magnetic fields and specialized perfusion probes as demonstrated by Flint *et al.* in this report. This represents an early but critical step in determining the influence of the underlying cellular mechanisms that lead to signal changes in an fMRI scan.

• This work was published in *Neuroimage 2009 (March 12 Epub ahead of print)*.

MR Microscopy of Neuronal Activity in Brain Slices

J.J. Flint (UF, Neuroscience), B. Hansen (Arhus University, Denmark), P. Vestergaard-Poulsen (Arhus University, Denmark), S.J. Blackband (UF, Neuroscience)

INTRODUCTION

fMRI has become the leading modality for studying the working brain. Being based on measuring the haemodynamic changes after enhanced mass neuronal activity, the spatiotemporal resolution of the method is somewhat limited. However, it remains unclear whether signal changes observed with fMRI methods reflect cell swelling related to neural activation, residual vascular effects, or a combination of both. In these studies, we present evidence of a detectable activity-related change in the diffusion weighted MR-signal from the cellular level in live hippocampal slices developed for MR by our group[1] in the absence of blood. Slices are exposed to several substances that elicit or inhibit neural activity and the effects evaluated and compared. The results were also compared to earlier DW fMRI studies in humans.
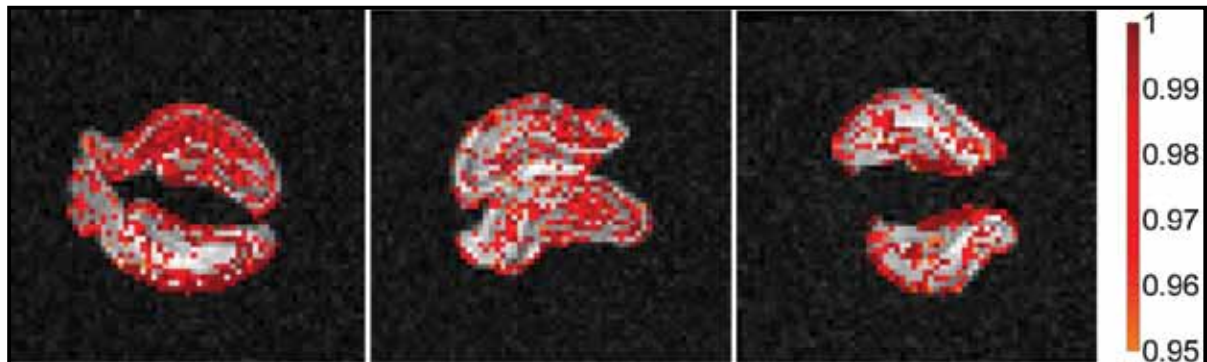
Figure 1.
Difference maps on six brain slices showing significantly different pixels (red, overlaid on grayscale MR images) between the resting state and active state (after kainate) at b = 2400 s/mm^2.

EXPERIMENTAL

Diffusion-weighted images 600 MHz (14.1 tesla) Bruker MRI system. After establishing a baseline, isolated rat brain slices samples were perfused with ACSF containing a compound intended to evoke neural activity (27mM KCl or 10μM kainate). Osmolality of the ACSF solutions was maintained at physiological levels by removal of equimolar amounts of NaCl. Lastly, perfusion was interrupted before running the imaging protocol (30 min) a second time. In experiments that employed chemical inhibition, the inhibitor (10μM MK-801 or 10μCNQX) was present in the ACSF as well as the tissue cutting medium as previous studies have shown increased efficacy with pretreatment. All experiments were carried out with a bore temperature matching the ambient temperature of 23° C.

RESULTS AND DISCUSSION

After baseline data demonstrated the stability of the slices, both stimulating chemicals elicited signal changes, with the kainite results shown in Figure 1. Differences in the signal distribution are considered in terms of differences in the mechanism of the excitatory compounds. Both of the inhibiting chemicals reduced the effects.

CONCLUSIONS

These data show chemical stimulation and inhibition of neuronal activity in brain slices where blood flow is excluded. This enables the examination of the origins of fMRI signal changes in tissues. The signal changes are attributed to micro-structural changes occurring at the cellular level. With sufficient development, this effect could be employed in functional neuroimaging experiments that obtain better spatial and temporal resolution than offered by current MEG and BOLD-based protocols. This work has now been published[2]. In order to elucidate mechanism, we have also embarked on MR studies at the cellular level, reporting for the first time MR images of mammalian neurons (rat) with direct histological validation[3]. By extension to *in vivo* studies, and looking at MR signal changes with functional stimulation, the origins of DW fMRI measurements may be addressed.

ACKNOWLEDGEMENTS

REFERENCES

1. T.M. Shepherd, S.J. Blackband, E.D. Wirth III, *Magn Reson Med*, **48**(3):565-569 (2002).
2. J.J. Flint *et al., Neuroimage 2009 (Feb 20 Epub ahead of print)*.
3. J.J. Flint *et al., Neuroimage 2009 (March 12 Epub ahead of print)*.

LIFE SCIENCES

CHEMISTRY

The high-field (≥9.4 tesla), high resolution Fourier transform ion cyclotron resonance (FT-ICR) mass spectrometers at the Magnet Lab are unique in their mass accuracy and resolution capabilities. These capabilities are used to resolve and identify thousands of elemental composition from highly complex mixtures such as petroleum, and have created the field of petroleomics. Applications include molecular weight distribution, distillation profile, characterization of specific fractions without prior extraction or wet chemical separation from the original bulk material, biodegradation, maturity, water solubility (and oil:water emulsion behavior), deposits in oil wells and refineries, efficiency and specificity of catalytic hydroprocessing, "heavy ends" (asphaltenes) analysis, corrosion, etc. This unique data can be used to increase discovery, production and refining of petroleum and petroleum products.

• This research was published in the *Proceedings of the National Academy of Sciences, U.S.A.*, **105**, 18090-18095 (2008).

Petroleomics: Chemistry of the Underworld

A.G. Marshall (FSU, Magnet Lab, Chemistry); R.P. Rodgers (FSU, Magnet Lab)

RESULTS AND DISCUSSION

Each different molecular elemental composition, $C_c H_h N_n O_o S_s \cdots$, has a different exact mass. With sufficiently high mass resolving power ($m/\Delta m_{50\%} \approx 400{,}000$, in which m is molecular mass and $\Delta m_{50\%}$ is the mass spectral peak width at half-maximum peak height) and mass accuracy (<300 ppb) up to ~800 Da, now routinely available from high-field (≥9.4 T) FT-ICR MS at Magnet Lab, it is possible to resolve and identify uniquely and simultaneously each of the thousands of elemental compositions from the most complex natural organic mixtures, including petroleum crude oil. It is thus possible to separate and sort petroleum components according to their heteroatom class ($N_n O_o S_s$), double bond equivalents (DBE = number of rings plus double bonds involving carbon, because each ring or double bond results in a loss of two hydrogen atoms), and carbon number. "Petroleomics" is the principle that from sufficiently complete characterization of the organic composition of petroleum and its relatives and products, it should be possible to correlate (and ultimately predict) their properties and behavior. Examples include molecular weight distribution, distillation profile, characterization of specific fractions without prior extraction or wet chemical separation from the original bulk material, biodegradation, maturity, water solubility (and oil:water emulsion behavior), deposits in oil wells and refineries, efficiency and specificity of catalytic hydroprocessing, "heavy ends" (asphaltenes) analysis, corrosion, etc. Figure 1 shows a portion of the first "petroleome" for just the species containing one sulfur atom (plus carbon and hydrogen) –– remarkably, nature has generated virtually all possible elemental compositions of this compound class, up to ~50 carbons.
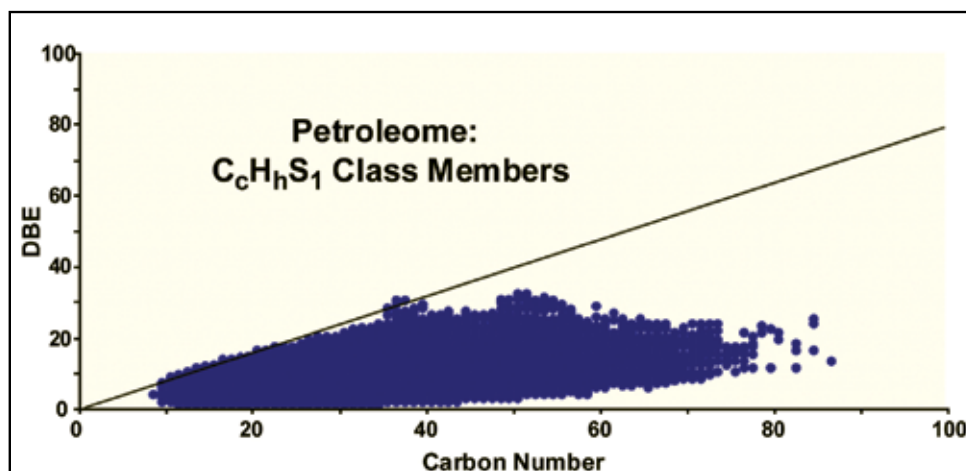
Figure 1.
Plot of number of rings plus double bonds (double bond equivalents = DBE, a measure of aromaticity) vs. number of carbons for all organic molecules containing carbons, hydrogens, and one sulfur atom identified to date in dozens of petroleum crude oil samples. The diagonal line indicates the maximum possible DBE. Note that nature has filled virtually all of the possible "compositional space" in the 70 million years during which the oil was formed.

ACKNOWLEDGEMENTS

REFERENCES
1. A.G. Marshall *et al.*, *Proc. Natl. Acad. U.S.A.*, **105**, 18090-18095 (2008).

CHEMISTRY

Polymorphism is the ability of a drug to exist in different crystalline environments, with potentially important consequences for stability (spontaneous conversion into metastable forms). Polymorphs also exhibit different melting points, solubilities (which affect the dissolution rate of drug and consequently its bioavailability in the body). In this report $^{35}Cl^-$, which is a common counterion in drugs, is used to monitor polymorphism by means of solid-state nuclear magnetic resonance (SSNMR) with a magic-angle spinning (MAS) probe and flat coil HX static probe at the Magnet Lab's Ultra Wide Bore 900 MHz spectrometer. The ^{35}Cl NMR spectra of mexiletine HCl drug of 2 different polymorphs were obtained and modeled by quantum-chemical calculations.

Application of Solid-State ^{35}Cl NMR Spectroscopy for the Detection of Polymorphism in a Variety of Hydrochloride Pharmaceutical Drugs

Hiyam Hamaed (University of Windsor (UW), Windsor, Ontario, Canada), Mike Laschuk (UW), Riqiang Fu (Magnet Lab), and Robert W. Schurko (UW)

INTRODUCTION

^{35}Cl solid-state NMR (SSNMR) spectroscopy is a powerful complimentary technique to XRD and ^{13}C SSNMR experiments for the study of pharmaceutical polymorphs. It provides clear information on the number of chlorine sites and shows great utility for identifying sites in non-crystalline, disordered or even impurity phases, especially in cases where the solid-state ^{13}C NMR spectra or powder XRD data are unable to differentiate polymorphs. Due to the usefulness of the ^{35}Cl SSNMR in identifying different polymorphs and the fact that 50% of all pharmaceutical salts are HCl salts and that chlorine is present ca. 25% of drugs, we are extending this work to include a variety of HCl pharmaceuticals and their polymorphs. The use of ultra-high-field NMR spectrometers is crucial for the success of such work, for both fast acquisition of high *S/N* NMR spectra and accurate determination of anisotropic quadrupolar and chemical shift parameters. In this project, we utilized ^{35}Cl SSNMR spectroscopy, at 9.4 and 21.1 (T) tesla, to study a number of HCl pharmaceuticals. The sensitivity of the ^{35}Cl chemical shielding (CS) and electric field gradient (EFG) tensors to subtle changes in the Cl environments is reflected in the ^{35}Cl SSNMR powder patterns. When coupled with standard ^{13}C and ^1H NMR experiments, XRD and *ab initio* calculations of NMR parameters, ^{35}Cl SSNMR is a powerful probe of HCl pharmaceuticals and their polymorphs.
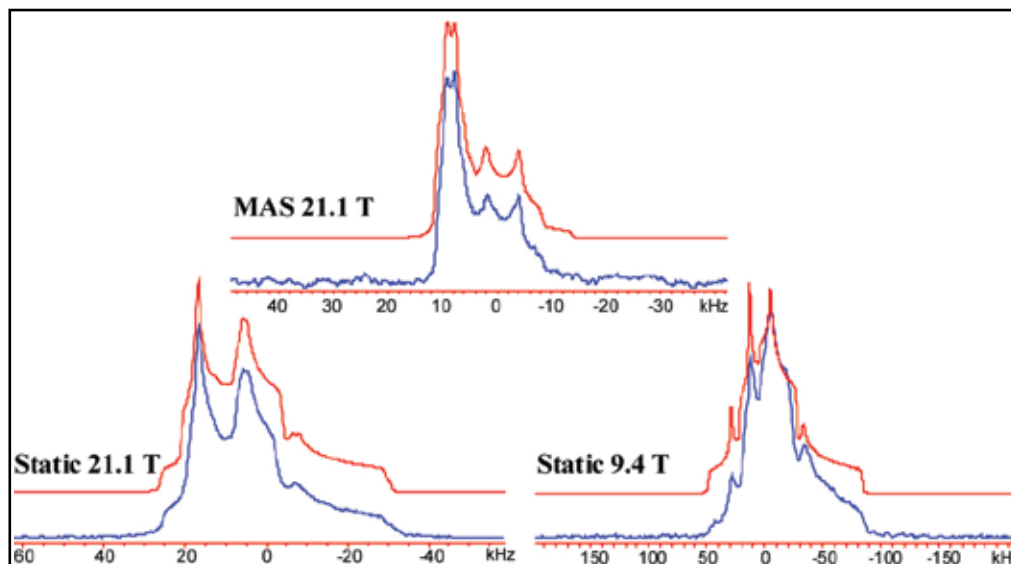
Figure 1.
^{35}Cl MAS and static NMR spectra and simulations of mexiletine HCl at two different fields

EXPERIMENTAL

^{35}Cl SSNMR experiments were carried out on a Varian Infinity Plus spectrometer with an Oxford 9.4 T wide-bore magnet using 5 mm HX static probe at the University of Windsor. High field ^{35}Cl NMR data were collected on the Ultra Wide Bore 900 MHz (21.1 T) superconducting NMR magnet at the Mag Lab using a 3.2 mm MAS HX probe and flat coil HX static probe.

CHEMISTRY

RESULTS AND DISCUSSION

The ^{35}Cl NMR spectra of mexiletine HCl (MH) (Figure 1) reveal two different chlorine sites, in agreement with the crystal structure. Experiments at 21.1 T are crucial for (i) obtaining high-resolution MAS NMR patterns and (ii) isolating anisotropic CS parameters. Simulations reveal quadrupolar coupling constants, C_Q, of 5.45 & 3.1 MHz, and asymmetry parameter, η_Q, of 0.40 & 0.55 for the two sites. The ^{35}Cl NMR spectra of two polymorphs of MH, which have no known crystal structures, were also obtained. ^{35}Cl NMR spectra of MH polymorphs show very different chlorine environments; modeling with *ab initio* calculations should provide much insight into their structures.

CONCLUSIONS

The sensitivity of the ^{35}Cl EFG and CS tensor parameters to the chlorine environments, and the potential to model these sites with *ab initio* calculations, holds much promise for application to a wide variety of HCl pharmaceuticals.

SUMMARY

Hydrochloride local anesthetic (LA) compounds are a group of drugs with common structural features that allow conformational flexibility (related to pharmaceutical function and activity) in their structures that lead to the possibility of formation of different polymorphs, as well as hydrates and solvates (pseudopolymorphs). We demonstrate in this research that ultra-high-field ^{35}Cl SSNMR is critical for obtaining high S/N ^{35}Cl NMR spectra and accurately determining ^{35}Cl anisotropic quadrupolar and chemical shift parameters from different polymorphs. This study represents the first application of ^{35}Cl SSNMR for the structural characterization and identification of polymorphism in solid pharmaceuticals.

ACKNOWLEDGEMENTS

MLR

Cotten *et al*. have taken advantage of the spectral resolution enhancement of the HETCOR (*het*eronuclear *cor*relation) spectra that is achievable at 900 MHz to study the ^{15}N-backbone labeled amidated piscidin 1 peptide. They found that the resolution of high resolution HETCOR spectroscopy is increased by 150% for both ^{1}H and ^{15}N dimensions when moving from 600 to 900 MHz. This increase in spectral resolution is important in the structural studies of multiply or uniformly labeled membrane bound proteins and peptides.

Enhancing Spectral Resolution of Dipolar-Encoded HETCOR Spectra at 900 MHz

Riqiang Fu (Magnet Lab); Daniel J. Hibbard (Pacific Lutheran University); Myriam Cotten (Hamilton College)

INTRODUCTION

High resolution HETCOR spectroscopy[1] has recently been developed to obtain orientational restraints (i.e., both the anisotropic ^{1}H and ^{15}N chemical shifts and their ^{1}H-^{15}N dipole-dipole couplings) from membrane proteins in a lamellar phase lipid environment. The HETCOR resonances of an ideal α-helical structure form characteristic wheels. Similar to PISA wheels (*p*olarity *i*ndex *s*lant *a*ngle)[2] the size and position of these wheels in the spectra can be used to uniquely determine the helical tilt with respect to the bilayer normal without resonance assignments. In this report, we use a multiple ^{15}N-backbone labeled amidated piscidin 1 (p1) peptide oriented in hydrated 3:1 DMPC/DMPG bilayers to illustrate the spectral resolution enhancement of the HETCOR spectra at high fields.

EXPERIMENTAL

The ^{1}H-^{15}N HETCOR experiments were performed on an ultra-wide bore superconducting 21.1 T magnet with a Bruker Avance 900 NMR console. High resolution ^{1}H chemical shifts were evolved in the t_1 dimension with high power ^{1}H homonuclear decoupling, followed by a short isotropic mixing time to ensure that the ^{15}N magnetization observed in the t_2 dimension was transferred from its closest ^{1}H. With the presence of ^{15}N decoupling in the t_1 dimension, only the ^{1}H chemical shifts are evolved, resulting in typical ^{1}H-^{15}N HETCOR spectra. On the other hand, with the absence of ^{15}N decoupling in the t_1 dimension, the ^{1}H chemical shifts are encoded by the ^{1}H-^{15}N dipolar interaction, leading to the dipolar-encoded HETCOR (or de-HETCOR) spectra.

CHEMISTRY

RESULTS AND DISCUSSION

Figure 1 shows the 2D ^1H-^{15}N correlation spectra of a 10-site ^{15}N labeled p1-NH$_2$ peptide oriented in 3:1 DMPC/DMPG bilayers. Out of 10 resonances, nine are identified in the HETCOR spectrum (Figure 1A).
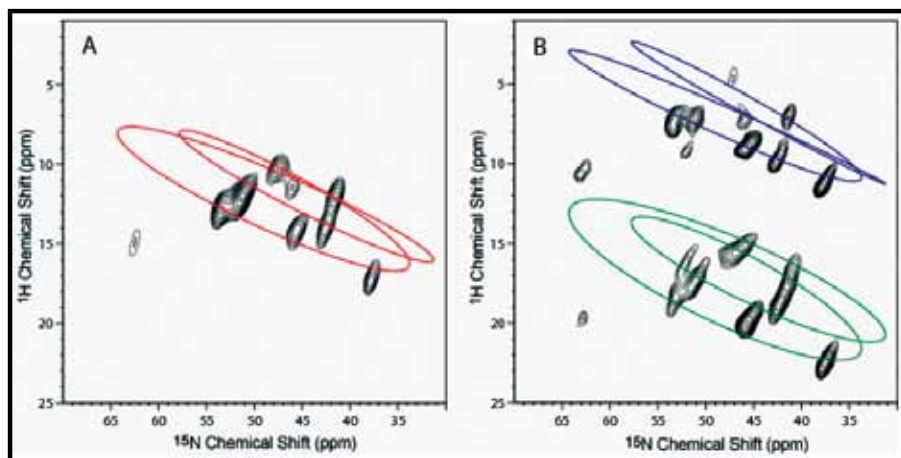
Figure 1.
2D ^1H-^{15}N correlation spectra of a 10-site ^{15}N labeled piscidin 1 peptide oriented in lipid bilayers recorded on the ultra-wide-bore 900 MHz NMR spectrometer. A) HETCOR. B) de-HETCOR. The curves were simulated with a MATLAB program using ^{15}N and ^1H chemical shift tensors in an ideal α-helix with a tilt of 86º with respect to the magnetic field.

In the de-HETCOR spectrum (Figure 1B), the resonances are split into two distinct groups due to the dipolar couplings. For the upper group, 10 resonances are observed, implying that the overlapped resonances at ~52 ppm in the ^{15}N chemical shift region of the HETCOR spectrum can be resolved in the de-HETCOR spectrum. Figure 2 shows the ^1H and ^{15}N slices taken from the de-HETCOR spectra at different static field strengths for the ^{15}N resonance at 37.8 ppm. Clearly, by going from the 600 to 900 MHz, the spectral resolution in both the ^1H and ^{15}N dimensions improves by ~150%. Therefore, with improved spectral resolution at higher magnetic fields, the 2D de-HETCOR spectra, allowing for simultaneous extraction of anisotropic ^1H and ^{15}N chemical shifts as well as their dipolar couplings, would become valuable in the structural studies of multiply or uniformly labeled membrane bound proteins and peptides.

ACKNOWLEDGEMENTS

Figure 2.
^{15}N and ^1H slices taken from the de-HETCOR spectra recorded at different fields for the resonance at the ^{15}N chemical shift of 37.8 ppm. A and C) the ^{15}N and ^1H slices from a Bruker Avance 600 MHz NMR spectrometer; B and D) the ^{15}N and ^1H slices from the ultra-wide bore 900 MHz NMR spectrometer.
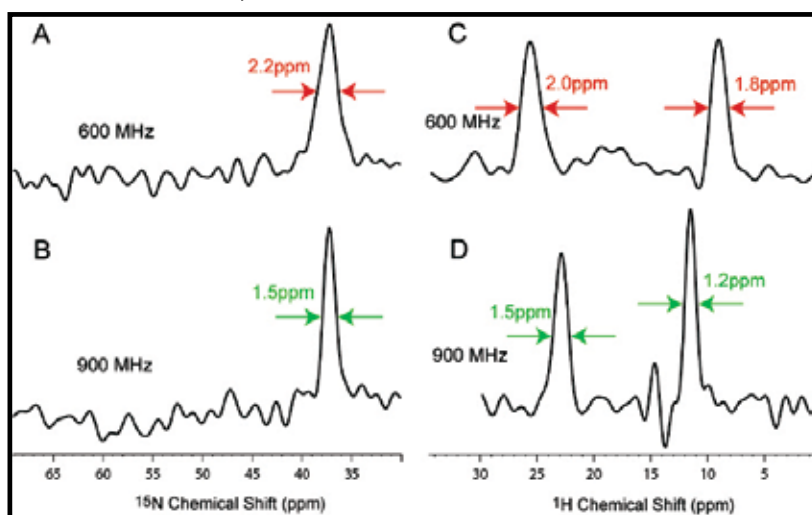
REFERENCES
1. R. Fu *et al.*, *J. Magn. Reson.*, **188**, 41 (2007).
2. J. Wang *et al.*, *J. Magn. Reson.*, **144**, 162 (2000); F.M. Marassi and S.J. Opella, *J. Magn. Reson.*, **144**, 150 (2000).

CHEMISTRY

Solid-state nuclear magnetic resonance of low–γ nuclei is challenging due to the intrinsic low-sensitivity. This report presents the development for enhancing sensitivity of low–γ quadrupolar nuclei and especially for the multiple-quantum magic-angle spinning (MQMAS) experiment. These methods includes a high B_0 magnetic field, an efficient probe using a balanced circuit for generating high B_1 magnetic field, and an optimal MQMAS sequence. High B_0 and B_1 magnetic fields and efficient pulse sequences can provide the critically needed sensitivity for low–γ quadrupolar nuclei. The technology development effort has been submitted for publication to Journal of Magnetic Resonance.

• The user science enabled by this technology and discussed in this report was published in *Science*, **321**, 113-117 (2008).

Enhancing MQMAS of Low-γ Quadrupolar Nuclei using High B_0 and B_1 Fields

Zhehong Gan, Peter Gor'kov, William Brey (Magnet Lab); Paul J. Sideris, Clare P. Grey (SUNY StonyBrook)

INTRODUCTION

Many quadrupolar nuclei, such as ^{25}Mg, ^{39}K, ^{43}Ca, ^{45,47}Ti, ^{67}Zn, ^{73}Ge, ^{95,97}Mo and ^{99,101}Ru, that can be exploited for the structural study of glasses, minerals, catalysts, ceramics and semiconductors, have very low gyro-magnetic ratio γ. Solid state NMR of these low–γ nuclei is challenging due to the intrinsic low-sensitivity. This report presents two recent developments for enhancing sensitivity of low–γ quadrupolar nuclei and in particular for the MQMAS experiment. These methods include an efficient probe using a balanced circuit for generating high B_1 magnetic field, an optimal MQMAS sequence, both in conjunction with a high B_0 magnetic field,.

EXPERIMENTAL

All measurements were performed using a 19.6 tesla (830 MHz) narrow bore instrument at the Magnet Lab with a lab-built 4-mm MAS probe.
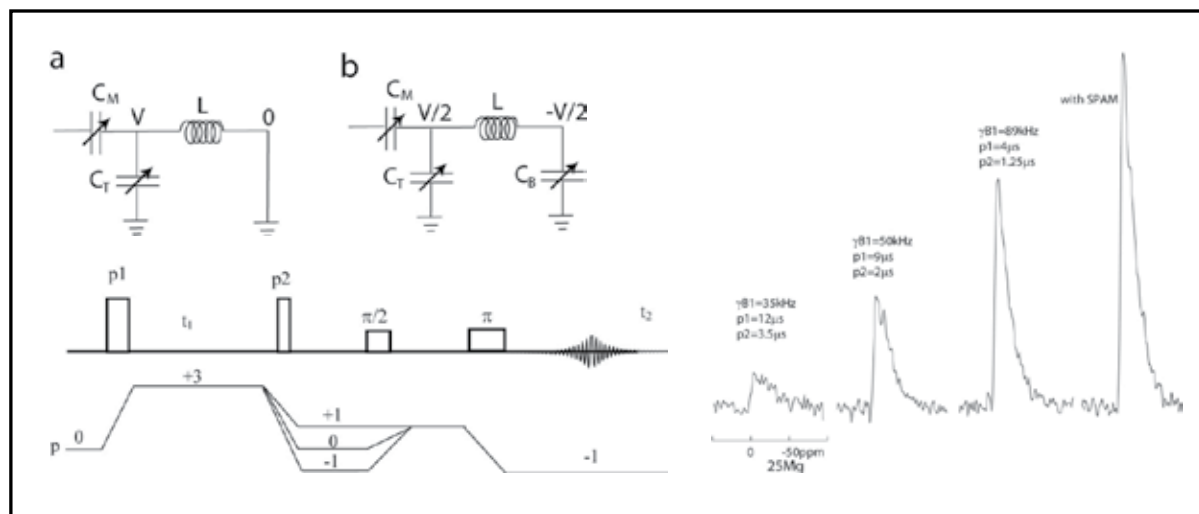
Figure 1.
(top left) conventional and balanced resonant circuit, (bottom left) SPAM-MQMAS pulse sequence and (right) ^{25}Mg MQMAS sensitivity enhancement using a 19% Al-doped Al/Mg Layered-Double-Hydroxide sample.

RESULTS AND DISCUSSION

The widely used 2D MQMAS experiment is a powerful tool for the study of quadrupolar nuclei[1]. The efficiency of MQMAS is far from ideal and highly dependent on the *RF* magnetic field strength B_1. Figure 1 shows a balanced circuit that can quadruple the power handling of an NMR probe and double the B_1 field that can achieved. A conventional resonant circuit consists of one tuning capacitor *C* and sample coil *L*. The B_1 field is typically limited by the maximum voltage *V* that can be supported before arcing occurs across the capacitors. The balanced circuit has two tuning capacitors that split the voltage to *V*/2 and −*V*/2 with the middle point of the coil at a virtual ground. This simple modification effectively reduces the peak voltage by factor of 2 and enables the doubling of *RF* field provided the availability of a sufficiently powerful

RF amplifier. Selection of the MQMAS pulse sequence is also important. The shifted-echo experiment has better efficiency than the *z*-filtered version, and is therefore preferred for low–γ quadrupolar nuclei[2]. Figure 1 shows the recently introduced *s*oft-*p*ulse-*a*dded-*m*ixing (SPAM) shifted-echo pulse sequence that can enhance the MQMAS by approximately 50% by simply adding a central-transition selective 90° pulse before the shifted-echo[3]. A gain in sensitivity nearly an order of magnitude by using the high B_1 field and the optimized pulse sequence has been demonstrated for ^{25}Mg MQMAS NMR of a Layered Double Hydroxide (LDH) sample[4]. A ^{25}Mg MQMAS spectrum of a 33% Al-doped sample recently provided key evidence of Al/Mg ordering in LDH materials[5].

CONCLUSIONS

The use of high B_0/B_1 magnetic field and optimal pulse sequence can dramatically enhance the sensitivity of MQMAS experiment. The compounded sensitivity gain can extend the powerful MQMAS experiment to insensitive low-γ quadrupolar nuclei, even for those with low natural abundance[6,7].

REFERENCES
1. L Frydman, J.S. Harwood, *J. Am. Chem. Soc.*, **117**, 5367-68 (1995).
2. D. Massiot *et al.,* SSNMR, **6** (1996) 73-83.
3. Z.Gan, H.Kwak, *J. Magn. Reson*., **168**, 346-51 (2004).
4. Z. Gan *et al., J. Magn. Reson,*. Submitted.
5. P.J. Sideris *et al.,* Science **321**, 113-117 (2008).
6. M. Davis *et al., Phys. Chem. Chem. Phys*., submitted.
7. P.J. Sideris *et al.,* manuscript in preparation.

CHEMISTRY

MAGNET SCIENCE & TECHNOLOGY

The Magnet Lab has been actively participating in the study of nanomaterials in collaboration with other institutes. The authors report research on synthesis, characterization and function evaluation of nanoparticles that have the potential for medical applications, particularly for noninvasive imaging in combination with PAT and magnetic resonance imaging.

• This work was published in *Chemistry of Materials*, **20** (19), 6087-6094 (2008).

Gadolinium Doped Gold-Speckled Nanoparticles for Multimodal Imaging

P. Sharma, B. M. Moudgil, S. C. Brown (University of Florida, Materials Science and Engineering & PERC); N. Bengtsson, E. W. Scott (UF, Molecular Genetics and Microbiology); Q. Zhang, H. Jiang (UF, Biomedical Engineering); S. R. Grobmyer (UF, Surgery); S. Santra (UCF, NanoScience, Chemistry and Biomolecular Science Center); G.A. Walter (UF, Physiology and Functional Genomics)

INTRODUCTION

Clinically used imaging modalities such as computed tomography, magnetic resonance imaging (MRI), ultrasound etc. do not provide complete structural and functional information independently. It is thus advantageous to obtain information from complimentary imaging modalities to facilitate diagnosis. This has lead to the development of multimodal contrast agents, which can generate contrast simultaneously from desired imaging modalities[1]. Herein, we describe the synthesis, characterization and functional evaluation of a new class of gold-silica hybrid nanoparticles termed as gold speckled silica (GSS) nanoparticles. The multitude of dielectric-metal interfaces created by this method gives rise to unique photothermal properties that enable the use of these materials as contrast agents in photo acoustic tomography (PAT). Furthermore, the incorporation of gadolinium (Gd) into the silica matrix produces a multimodal GSS contrast agent for both magnetic resonance (MR) and PAT-based imaging. These multimodal particles are a novel step forward toward integrating multimodal detection and therapeutic capabilities into a single entity.

EXPERIMENTAL

The one pot, microemulsion mediated synthesis and characterization of Gd doped GSS nanoparticles has recently been published in detail elsewhere[2]. The dual imaging capabilities of these particles has been demonstrated using phantoms and *in vitro* studies. The MR data (T_1, T_2 and T_2*) was collected using a 4.7 tesla Bruker Avance MR scanner (AMRIS facility, UF). Relaxivity measurements were carried out in glass micropipettes filled with ~100 μL of serially diluted GSS nanoparticles (in 0.5% agarose) using 0.5% agarose as control. PAT measurements were made using a mechanical scanning photoacoustic system with single acoustic transducer using a pulsed Nd:YAG laser working at 532 nm with 4 ns pulse duration, 10 Hz repetition rate. The dual contrast generating ability of the GSS nanoparticles was demonstrated by injecting them in phantom (prepared using Intralipid, India ink, distilled water, and 2% agar powder) and consecutively imaging by MRI and PAT.

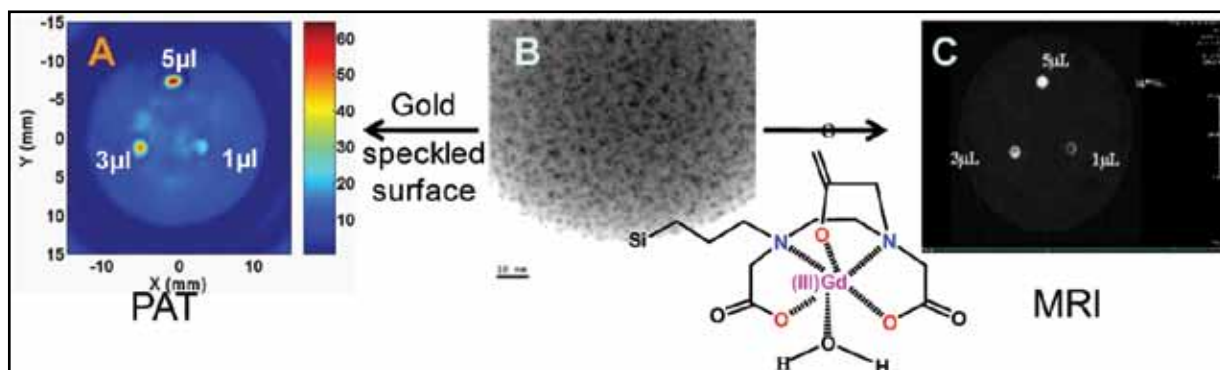**Figure 1.**
The TEM of the GSS nanoparticles (B) of ~100nm diameter; (A) and (C) show the PAT and MRI contrast from same phantom containing GSS nanoparticles.

RESULTS AND DISCUSSION

TEM of GSS nanoparticles (Figure 1, B) shows the surface layer of these nanoparticles is composed of discontinuous, irregular gold nanodomains of varying crystallinity incorporated within the supporting silica

matrix. Figure 1 A and C show the PAT and MRI (T_1) contrast from the same phantom containing 1, 3, and 5 µL (particle concentration, 10 mg/mL) of Gd-doped GSS nanoparticles. The relaxivities R_1, R_2, and R_2* have been determined to be 13, 110, and 173 mM^{-1} s^{-1}, respectively, which is much higher than commercially available contrast agents[2].

CONCLUSIONS

Gd doped GSS have been demonstrated as single nanoparticle contrast agent for non-invasive imaging by PAT and MRI. The optical absorption property of these particles also enables their use for photothermal applications.

ACKNOWLEDGEMENTS

REFERENCES

1. P. Tallury *et al.*, *Nanomedicine*, **3(4)**, 579-592 (2008).
2. P. Sharma *et al.*, *Chemistry of Materials*, **20(19)**, 6087–6094 (2008).

In what can be called an intersect between art and state-of-the-art, a new magic angle spinning (MAS) probe was developed for the solid-state NMR program. This design defines the edge of the envelope for both signal-to-noise ratio and heating. It uses a low electric (low-E) field configuration, pioneered by this team, in a MAS stator specially designed to fit a longer coil. The reduced heating, a result of lower electric fields, makes study of biological samples possible without destroying them. The coil aspect ratio increases sample volume without reducing spinning speed. The probe's excellent homogeneity on the 1H irradation channel is being exploited by Joanna Long and Seth McNeill to improve a key building block for NMR experiments: the inversion pulse. The probe and initial spectra have been published and the pulse development work will be published later. It can be expected that this design will slowly transition to the commercial sector.

• This work was published in *J. Magn. Reson.*, **197**, 135-144 (2009).

Experimental Optimization of Magic Angle Spinning Solid State NMR Spectroscopy at 750 MHz

S. McNeill (UF Electrical and Computer Engineering); P.L. Gor'kov, W.W. Brey (Magnet Lab/FSU); J.R. Long (UF Biochemistry and Molecular Biology)

INTRODUCTION

Solid-state NMR is uniquely suited to study peptide and protein structure and dynamics in heterogeneous systems under in situ conditions. However, new pulse techniques and RF probes are required to take full advantage of high magnetic fields available at the Magnet Lab. We have developed a 750 MHz MAS probe[1] based on the "low-E" crossed coil configuration previously demonstrated for static samples[2]. By using a specially designed stator housing (Figure 1) to provide an extra long slot for the sample, we have been able to increase sample volume to improve sensitivity. The low-E approach produces ^{1}H and ^{13}C RF magnetic fields with outstanding homogeneity (Figure 2), high efficiency, and reduced sample heating. The probe is being used for several applications, including double quantum recoupling experiments, which greatly benefit from the increased homogeneity.

Figure 1.
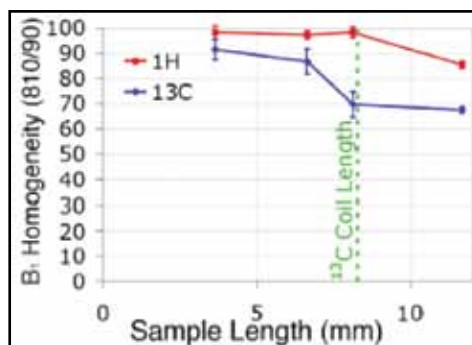A drawing of the stator and coil assembly.

Figure 2.
^{1}H (red) and ^{13}C (blue) B$_1$ homogeneity of the probe for different sample lengths.

METHODS

Simple rectangular pulses do not perform well at high fields due the increased effect of isotropic and anisotropic chemical shifts[3], so we designed composite pulses both to invert and refocus magnetization

MAGNET SCIENCE & TECHNOLOGY

over the widest possible bandwidth. We used the SPINEVOLUTION computer program to simulate frequency profiles[4] and the Nelder-Mead simplex method as implemented in Matlab to optimize the phases and lengths of segments of the composite pulses. The optimized pulses were then tested experimentally using the low-E probe.
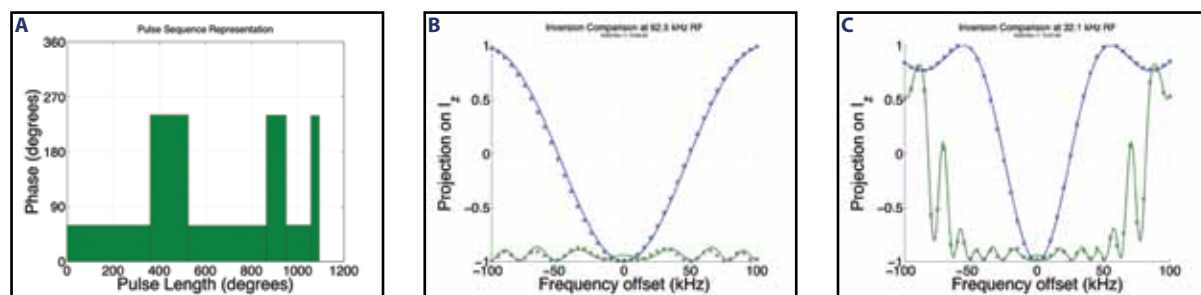
Figure 3

a) The phases and pulse lengths for a composite ^{13}C inversion pulse optimized for 750 MHz MAS spinning at 10 kHz using constant RF power at 50 kHz. b) Experimental (Xs) and simulated (line) data for a single 180º pulse (blue) and the optimized composite pulse (green) at 32 kHz RF power. c) Experimental (Xs) and simulated (line) data for a single 180º pulse (blue) and the optimized composite pulse (green) at 63 kHz RF power.

RESULTS AND DISCUSSION

Because the homogeneity of the probe on both the ^1H and ^{13}C channels is so high, it has not been necessary to include RF inhomogeneity effects in the model. This made the optimization routine simpler and the computations much faster. The Nelder-Mead simplex method worked well optimizing composite pulses having a small number (1-10) of elements with unconstrained pulse length and phase at constant RF power; good inversion with realistic experimental parameters can be found as shown in Figure 3. Note the remarkably good agreement between simulation and experiment. We are exploring the addition of further experimental constraints as well as other methods of optimization, such as genetic algorithms, to improve the quality of spectra from practical biological samples.

REFERENCES

1. S. A. McNeill *et al., J. Magn. Reson.*, **197**, 135-144 (2009).
2. P. L. Gor'kov e*t al., J. Magn. Reson.*, **185**, 77-93 (2007)
3. S. A. McNeill *et al., Magn. Reson. Chem.*, **45**, S209–S220 (2007).
4. M. Veshtort and R. G. Griffin, *J. Magn. Reson.,* **178**, 248-282 (2006).

Very large and very expensive high field superconducting magnets use cable-in-conduit conductor (CICC). The conduit is essentially a steel pipe for structural reinforcement, filled with a multi-strand cable of Nb_3Sn superconducting strands or wires in a cabling pattern that is still under development. These conductors play a major role in magnets for ITER, the large international experimental facility for the production of energy from fusion. The performance of these conductors has been studied in conductor test facilities such as Test ARrangement for Strain Influence on Strands (TARSIS) and in major ITER test coils, and shown to vary widely with the design of the cable. With the Florida electro-mechanical cable model (FEMCAM), the Magnet Lab has made an important contribution in explaining the low performance of earlier Nb_3Sn CICC conductor tests and can help finalize the CICC design for ITER. The model has played a major role in the design of the Series Connected Hybrid CICC magnets at the Mag Lab.

• This work has been submitted to *Cryogenics* and is under review.

Modeling of Nb_3Sn CICC Performance Degradation due to Strand Bending and Inter-filament Current Transfer

Y. Zhai (MS&T, Magnet Lab)

INTRODUCTION

The Florida electro-mechanical cable model (FEMCAM), previously benchmarked against 40 different conductor tests, is used to study the influence of bending strain and current non-uniformity on the critical current and n-value of Nb_3Sn strands and CICC cables. The new model predicts that critical current degradation of bent strands initially follows the curve of full inter-filament current transfer but starts deviating with large bending strain and falls between the curves of full current and no current transfer. The results are consistent with recent TARSIS measurements.

MODEL DESCRIPTION

The new numerical model combines thermal bending effects during cool-down, electromagnetic bending effects during magnet operation and resistive transition in strands with filament fracture. The thermal bending model is incorporated into an electromagnetic bending model that describes strand mechanical interactions in a CICC by bending of clamped beams and contact stress at strand crossing. The total bending strain is used to compute transverse load degradation from the Summer scaling law and Ekin integration. We assume that filament critical current drops to zero if filament strain is greater than the strand irreversible limit.

RESULTS AND DISCUSSION

Figure 1 presents correlation of the FEMCAM predicted critical current degradation on the first cycle with various CICC tests. It also presents the FEMCAM simulated critical current and n-value reduction due to bending for the OST dipole strand used for the SCH CICCs.
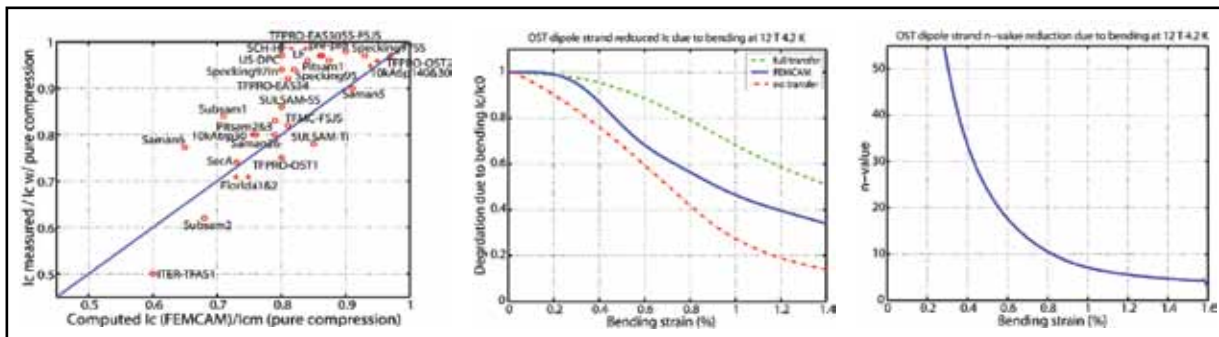

Figure 1. Correlation of FEMCAM with CICC tests. FEMCAM simulated critical current and n-value reduction due to bending for OST dipole strand.

CONCLUSIONS

FEMCAM simulated strand and cable n-values are compared with various CICC measurements. The results imply that FEMCAM is a useful tool for the design of Nb_3Sn-based CICCs and that both the thermal bending and the electromagnetic bending play important roles in CICC performance.

ACKNOWLEDGEMENTS

REFERENCES
1. Y. Zhai *et al.*, *IEEE Trans. Appl. Supercond.*, **18**, 1127-1130 (2008).
2. Y. Zhai *et al., Supercond. Sci. Technol.*, **21**, 115010, (2008).

Large-scale fusion reactors and high energy physics particle accelerators continue to demand higher and higher magnetic fields to effectively contain the plasma (fusion) or bend and focus the particle beam (accelerators). To do this, designers are increasingly turning to Nb_3Sn, a brittle intermetallic superconductor that can carry a lossless electrical current at fields up to 25 tesla. However, the material is inherently brittle, and the very large magnetic forces exerted on the magnet conductor during operation can cause the individual superconducting filaments to crack, rendering them useless. By developing advanced sample preparation techniques, this project shows how these cracks can be imaged directly, and how the architecture of the superconducting wire can be manipulated to make the filaments tougher and more resistant to cracking.

Fracture Behavior of ITER and HEP-style Nb_3Sn Superconducting Strand

M.C. Jewell (Magnet Lab), P.J. Lee (Magnet Lab), D.C. Larbalestier (Magnet Lab)

INTRODUCTION

Large-scale science projects such as ITER (an international net-energy nuclear fusion reactor being built in southern France) and high energy physics (HEP) particle accelerators require enormous superconducting magnets to generate the very large magnetic fields crucial to the success of the projects. One superconducting material of choice for these systems is the brittle intermetallic Nb_3Sn. Fabricated

MAGNET SCIENCE & TECHNOLOGY

MAGNET SCIENCE & TECHNOLOGY

in the form of a composite multifilamentary wire, Nb_3Sn strands can unfortunately be susceptible of the cable significantly reduces the performance of the machine over time. To understand the effect of strand architecture (filament size, spacing and arrangement) on fracture propensity, we have developed a metallographic technique to image Nb_3Sn strands in longitudinal cross-section after mechanical and/or electrical testing.

EXPERIMENTAL

To explore a wide range of strain states, deformation conditions included pure bending at 77 K, microindentation at room temperature, uniaxial tension at 4.2 K, and electromagnetic testing at 4.2 K (in collaboration with the University of Twente, The Netherlands). Sample cross-sections were polished both manual and by automatic (vibratory) polishing, and after subsequent chemical etching, the specimens were imaged using a field emission scanning electron microscope.

RESULTS AND DISCUSSION

Under bend strain, strands designed for low filament coupling (ITER) exhibit primarily individual filament cracking, with some collective cracking occurring in internal tin strands that have agglomerated filaments near the sub-bundle core. This cracking occurred primarily at local bend strain values above 0.7% for strands with reacted filaments of 3 – 4 μm diameter, and at local bend strain values above 0.4% for strands with reacted filaments of 6 μm diameter. In contrast, strands designed for maximum critical current density (HEP) exhibited long, collective cracks under bending that propagated across entire sub-bundles and even from sub-bundle to sub-bundle, beginning at the tensile bend axis and ending near the geometric neutral bend axis (see figure 1 and detail in figure 2). Additionally, the fracture morphology is shown to be constant for a wide variety of HEP strands, with critical current density values ranging from 1700 A/mm^2 to 3000 A/mm^2.
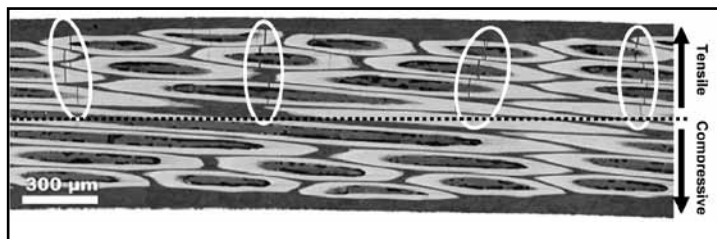

Figure 1.
High current strand bent to 1.5% strain at 77 K. The fracture morphology consists of long, discrete chains of cracks (highlighted here by white ovals) that propagate across sub-bundles, from the tensile axis to the neutral axis.
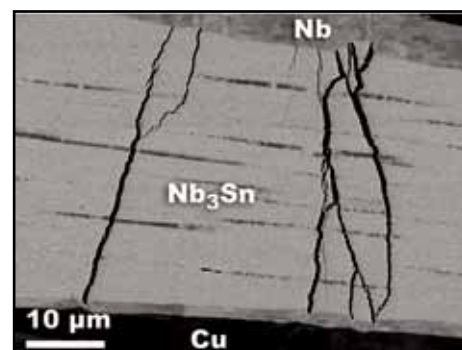

Figure 2.
Sub-bundle detail from Figure 1, showing the cracks propagating across multiple agglomerated Nb_3Sn filaments, effectively destroying the current-carrying capacity of the entire sub-bundle.

Under indentation testing, crack propagation was shown to be a strong function of the local strain state, with even small tensile stresses producing extended fracture fields, while indents in a region under compressive stress showed almost no fracture at all. The clear implication is that the local stress state is the most critical parameter to be controlled for preventing fracture in the conductor. These findings should provide significant guidance to the Nb_3Sn wire manufacturing community as they develop more fracture-resistant strands for magnet applications.

CONCLUSIONS

Fracture behavior in ITER-style strands with well-separated filaments can be influenced by strand design variables such as filament size and spacing. In high-J_c strands, however, such as those used in the Magnet Lab's Series Connected Hybrid magnet, fracture behavior is a function of the strain state imposed by the magnet conductor, and is insensitive to strand architecture variables, since the filaments largely agglomerate during heat treatment.

ACKNOWLEDGEMENTS

MAGNET SCIENCE & TECHNOLOGY

A new route to lower the AC loss and make fully decoupled filaments in YBCO coated conductors was proposed and implemented in prototype form. This advance addresses one of the key challenges of power applications of high-temperature superconductors in motors, generators and transformers. The method developed and implemented at the Magnet Lab has enabled a 10-fold reduction of AC losses in commercial YBCO coated conductors produced by the American Superconductor Corp. This significant AC loss reduction was achieved without mechanical twisting of the conductor.

• This work was published in *Superconductor Science and Technology*, **21**, 082004 (2008).

Significant Reduction of AC Losses in YBCO Patterned Coated Conductors with Transposed Filaments

Dmytro Abraimov (Magnet Lab), Alex Gurevich (Magnet Lab), Anatolii Polyanskii (Magnet Lab), X.Y. Cai (UW), Aixia Xu (Magnet Lab), Sastry Pamidi (FSU, Center for Advanced Power Systems), David Larbalestier (Magnet Lab) and C. L. H. Thieme (AMSC)

INTRODUCTION

The reduction of high hysteretic losses in high-T_c YBCO Coated Conductors (CC) tapes remains a very important and challenging problem for power applications of high-temperature superconductors in motors, generators and transformers. The usual way of reduction of AC losses by mechanical twisting of round wire multifilament conductors is practically impossible to apply to the thin film multilayer CC geometry. We proposed and implemented for the first time a new conductor design shown in Figure 1 (c), in which the transposed filaments are fully magnetically decoupled, thus providing a significant reduction of AC losses without mechanical twisting. This was accomplished using commercial YBCO coated conductors produced by American Superconductor Corp.

EXPERIMENTAL

The conductor consists of two patterned CCs with electrically insulated slanted filaments thermally bonded face to face through low-resistance bridges in the silver caps. The silver layers of each CC are partly covered by a thin dielectric layer, leaving two parallel uncovered conducting strips that only connect pairs of filaments from each conductor. CCs were patterned with three photolithography stages and wet chemical etchings and then thermally bonded together through resistive Ag bridges so that each filament is electrically connected with only two filaments in the other CC. The electrical conduction paths alternate along the tape in a zigzag pattern, providing complete filament decoupling. Magneto-optical imaging through W-Ni substrate has shown good filament alignment and good superconducting properties in all bonded samples.

RESULTS AND DISCUSSION

Our measurements have shown a 10-fold drop of AC losses in patterned samples with 0.5 mm wide filaments as compared to losses of the control sample for frequencies from 10 to 400 Hz. Detailed transport measurements on the patterned samples with reduced AC losses also revealed high critical current densities and low contact resistances in the range 2.4×10^{-8}–1.16×10^{-7} Ωcm^2.

CONCLUSIONS

We have implemented a new CC conductor architecture, which provides a significant reduction of AC losses in patterned CCs. The results of this work open up a possibility of a much more substantial loss reduction by further optimization of the bonding process and the reduction of the filament size.
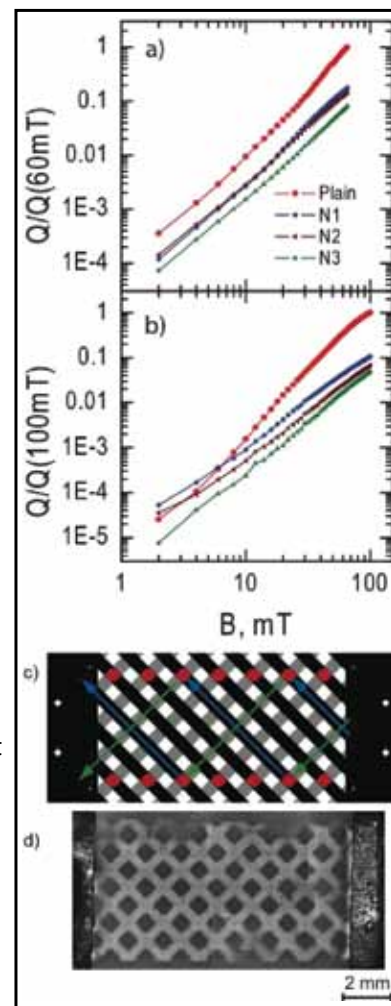
Figure 1.
Losses for three patterned samples at 400 Hz (a) and 55 Hz

(b) normalized to the maximum losses of the controlled sample.

(c) Sketch of two bonded CCs where the filaments in the top layer (black) and the bottom layer (gray) are only connected through the resistive silver bridges (red). Alternating current paths are shown with blue and green arrows.

(d) Magneto-optical image of trapped flux in a fully bonded conductor.

MAGNET SCIENCE & TECHNOLOGY

ACKNOWLEDGEMENTS

REFERENCES

1. D. Abraimov *et al.*, *Supecond. Sci. Technol.*, **21,** 082004 (2008).

The high temperature superconductor YBCO is also a very high field superconductor when operated at low temperature with tremendous promise to greatly extend the field range of superconducting magnets. The Magnet Lab took a significant step in the development of YBCO magnets with the demonstration of a record 33.8 tesla (T) in a small coil at very high current density. There is potential for YBCO based superconducting magnets to gradually replace the resistive user magnets at the Magnet Lab with savings in electric power costs while improving field stability and user access time.

33.8 Tesla with a YBa$_2$Cu$_3$O$_{7-x}$ Superconducting Test Coil

W.D. Markiewicz, K.W. Pickard, H.W. Weijers, P.D. Noyes, U.P. Trociewitz, J. Jaroszynski, A. Xu, D.C. Larbalistier (Magnet Lab)

A small coil wound of YBCO composite superconducting tape was tested in the DC field facility of the National High Magnetic Field Laboratory. In a background field of 31 tesla, the coil produced an incremental field of 2.8 T to reach a world record field of 33.8 T for the operation of a superconducting coil.

The superconductor YBCO is a type of high temperature superconductor, and is also a very high field superconductor when operated at the low temperature of liquid helium. YBCO conductors are being developed rapidly, motivated by potential application in the electric power industry. As a result of their low temperature properties, YBCO conductors are also expected to allow superconducting coils that operate at magnetic fields significantly higher than existing coils that use superconductors based on Nb technology. As an initial step in the development of a YBCO superconducting magnet technology, a small coil was made of a standard SuperPower tape conductor, 4.2 mm wide and having a Hastelloy substrate of 50 μm thick and a copper stabilizer thickness of 40 μm. The plan was to demonstrate coil performance at the highest practical field, which was provided by a 31 T resistive magnet with an available bore of 40 mm inside the insert cryostat. The coil, shown in Figure 1, is pancake wound, being constructed of five double pancakes with inner winding diameter 25 mm, outer winding diameter 36 mm, and assembled winding length of 46 mm. The pancakes are wound with 38 turns each with a total conductor length of approximately 36 m for the coil. With the background magnet at 31 T, the test coil was operated to increasing fields in 100 A increments. Voltages across the double pancakes were rather linear as a function of ramp current, indicating a lack of magnetic hysteresis and lack of shorting between turns or pancakes. It was observed that the temperature in the bore of the coil increased significantly during the ramps. This heating was attributed to a combination of the ohmic heating in the probe holding the test coil, and the fact that helium gas produced at this field level tends to accumulate in the bore due to the diamagnetic nature of helium and the strong
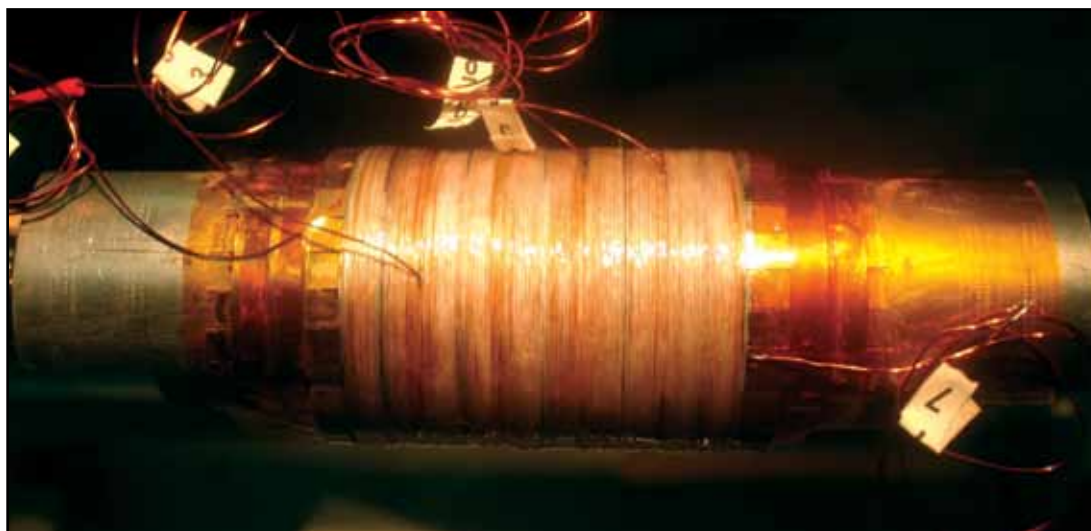

Figure 1.
33.8 T YBCO test coil, consisting of 10 pancakes with outer winding diameter 38 mm, winding length 46 mm, producing a field increment of 2.8 T in a 31 T background field, at a current density in the conductor of 756 A/mm^2.

field x field-gradient product present. The coil was operating in helium gas at increasing temperature during the ramps. The final ramp reached 325 A where the coil experienced a quench and was damaged. At this current, the average current density in the coil was 446 A/mm2, with an exceedingly high value of 756 A/mm2 for the current density in the conductor. The helium gas temperature surrounding the coil was estimated as exceeding 12 K, based on available measurements. During the quench, the coil was protected by a fast quench detector and an external discharge in a time on the order of 10 ms. The damage to the coil was attributed to mechanical effects. It is planned to rebuild the coil with increased reinforcement, and to modify the probe for structural rigidity as the first steps in a continuing program of coil technology development.

Nb-based magnets cannot supply fields of more than 22 tesla, about two-thirds of those possible with the 20 MW resistive magnets at the National High Magnetic Field Lab. In pursuit of parity of fields, we have been developing HTS conductors for very high field magnets, one route employing $Bi_2Sr_2CaCu_2O_{8+\delta}$ (Bi2212) round wire conductor. A small solenoid has recently been wound and tested in a field of 31 T generating a field increment of around 1 T thus becoming the first HTS wire-wound coil to reach beyond 30 T, the range in which the next generation of high field superconducting magnet systems is expected to operate.

Bi2212 Conductor and Coil Technology for High Field Magnets

U.P. Trociewitz, J. Jiang, T. Shen, F. Kametani, X. Liu, D. Myers, M. LoSchiavo, Y. Viouchkov, E.E. Hellstrom, H.W. Weijers, P. Noyes, J.L. Schwartz, and D.C. Larbalestier (ASC-Magnet Lab)

One of the goals of the Magnet Lab is to develop HTS magnet technology using $Bi_2Sr_2CaCu_2O_{8+\delta}$ (Bi2212) round wire conductor. A small solenoid has recently been wound and tested at a field of 31 T generating a field increment of around 1 T thus becoming the first HTS wire-wound coil to reach beyond 30 T, the range in which the next generation of high field superconducting magnet systems is expected to operate.

Figure 1.
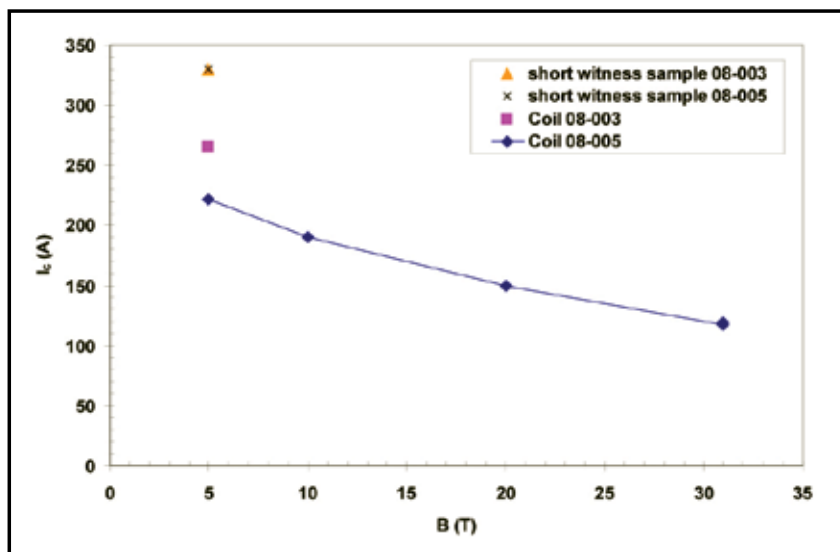View of the coil tested in 31 T background field.

Figure 2.
$I_c(B)$ data of the coil tested in 31 T background field (coil 08-005), a coil previously tested at 5 T (coil 08-003 with 32 mm ID, 56 mm OD, 10 layers, 90 mm high, 670 turns), and short 5 cm long witness samples.

With the need for ever higher magnetic fields and rising costs of energy, conventional magnet technologies, resistive as well as superconducting, are reaching their limits. Right now there are only three superconducting materials in technically applicable form available, whose transport properties show weak field dependence at high fields and reach far beyond 25 T, the physical limit of Nb_3Sn conductors: the tape conductors $YBa_2Cu_3O_{7-\delta}$ (YBCO) and $Bi_2Sr_2Ca_2Cu_3O_{10}$ (Bi2223), and round wire $Bi_2Sr_2CaCu_2O_{8+\delta}$ (Bi2212). Though transport properties of Bi2212 do not currently match YBCO, Bi2212 has particular technological relevance as it is available in round wire geometry and its full technological potential is not fully explored and is yet to be reached. As a driver for research and development of high field magnet technology using Bi2212 conductor, the concept of a 7 T insert magnet generating 25 T in 18 T background field has been developed, which builds on the experience gained during the previous 5 T insert coil program. The preliminary magnet design calls for a four-section layer-wound coil, each section having 10 layers, using round AgMg-alloy sheathed, braid-insulated

MAGNET SCIENCE & TECHNOLOGY

Bi2212 conductor (1.3 mm OD) employing a wind and react approach. After manufacturing, thermo-processing, and characterizing a series of small (10 layers, 12 turns) coils it became clear that before committing large amounts of conductor to a specific magnet design various questions need to be answered:

- Why are transport properties of coils consistently lower than transport properties of short samples?
- Does thermo-processing of solenoids with larger thermal mass affect transport properties?
- What is the in-field performance of wind-and-react layer wound coils?
- What is the practical stress limit of layer wound and epoxy impregnated coils?

In an effort to address these questions, several fully processed coils have been dissected and superconducting and microstructural properties of extracted short samples have been studied. It could be shown that coils up to a layer count of 15 can be processed yielding homogeneous properties throughout the layers. Recently a medium size coil has been manufactured and was tested in magnetic background fields up to 31 T using one of the resistive magnets at the Magnet Lab. The coil dimensions were ID = 15 mm, OD = 38 mm, h = 100 mm, with 10 layers, 75 turns, and a total conductor length of 66 m, figure 1. At 31 T this coil repeatedly generated an additional field of about 1 T without degradation making it the first HTS wire-wound coil to reach beyond 30 T, figure 2. Though the coil did not perform at its expected level it still reached a winding current density J_w of about 100 A/mm^2 surpassing J_w of the previous 5 T insert by more than 10%. It is suspected that one reason of the coils reduced performance was related to the small winding ID needed to operate the coil inside the small bore of the resistive outsert magnet. Further experiments are on the way to understand and develop magnet technology based on Bi2212 round wire.

The Magnet Lab in engaged in the continual upgrade of the user-available magnets of the Pulsed Field Facility. This prototype magnet has demonstrated improvements in technology that gave extended performance at more than 70 tesla in a capacitor driven science magnet. These improvements are being incorporated in the next generation of Magnet Lab pulsed magnets in a new design that will allow operation at 80 T.

- The science resulting from this research and development achievement has been published, Singleton, J. *et al.*, *Physica B: Physics of Condensed Matter*, **404**, 350-353 (2009).

70 T User Magnet Delivers 250 Pulses at Pulsed Field Facility

C.A. Swenson, J.R. Michel, J.E. Serna, M.D. Pacheco, A. Paris, M. Gordon and D.R. Rickel (Magnet Lab Pulsed Field Facility, Los Alamos)

INTRODUCTION

The Magnet Lab Pulsed Field Facility has completed its first science operations in a high-energy magnet user-cell available for science investigations. The first operational magnet in this cell is a modified 75 T coil assembly developed for the DOE-NSF 100 T Multi-shot Magnet Program. The cell was opened Dec. 10, 2007 after magnet refurbishment and an upgrade to the station and support instrumentation.

The station's primary scientific user was John Singleton who performed measurements of quantum Shubnikov de Haas oscillations at fields up to 72.5 T.

SUMMARY OF UPGRADE AND OPERATIONS

The magnet and station upgrade entailed the design and construction of secondary fault containment structures on both the coil and blast box assemblies. External Zylon containment rings were installed around the coil's mid-plain, electrical bus-feed, and lower electrical interconnect joint regions. The blast box assembly was also upgraded by installing spring loaded "Belleville" washers on all major fasteners to reduce the impulse loads on bolts during loading from shock waves. The Belleville washers were deemed necessary after earlier 80 T prototype testing in 2006.
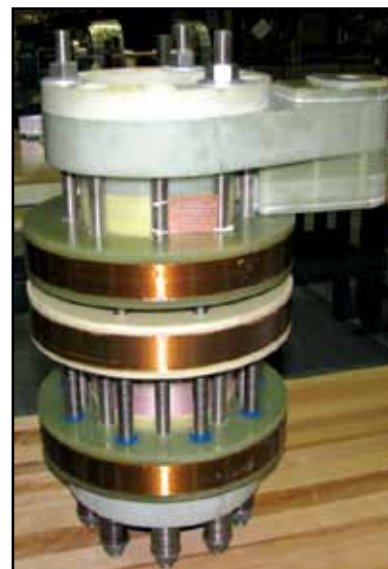

Figure 1.
Side view of 75 T magnet showing Zylon containment rings around coil assembly. The rings serve as secondary containment.

The two-coil magnet assembly was pulsed more than 70 T 253 times between December 2007 and March 2008. The external coil experienced an electrical fault without catastrophic structural failure. The internal coil of the magnet assembly experienced more than 350 pulses without internal electro-mechanical failure.

CONCLUSIONS

The 250 pulse performance of this prototype magnet has established the proof of principle for viable 70 T capacitor driven science magnets. The next generation of Mag Lab pulsed magnets will incorporate many of the design features developed for and tested by this prototype.

ACKNOWLEDGEMENTS

REFERENCES
1. Swenson, C.A. *et al., IEEE Trans. Appl. Supercond.*, **18 (2**), 604-607 (2008)
2. Swenson, C.A. *et al., IEEE Trans. Appl. Supercond.*, **16 (2**), 1650-1655 (2006)
3. Singleton J. *et al., Physica B: Physics of Condensed Matter*, **404**, 350-353 (2009)

MAGNET SCIENCE & TECHNOLOGY

CONDENSED MATTER PHYSICS

Geometrically frustrated $LuFe_2O_4$ is the poster child for fundamental studies of electronically driven multiferroicity. At the same time, the overall high energy scales and use of charge order to create a finite polarization that coexists with the ferrimagnetic state make it attractive for potential applications. This functionality and cross-coupling are the result of a delicate interplay between charge, structure and magnetism, interactions that Musfeldt *et al.* probe with comprehensive optical and Mossbauer spectroscopies, magnetization and x-ray studies.

• This work was published in *Physical Review Letters*, **101** (22), 227602 (2008).

Charge Order, Dynamics, and Magneto-structural Transition in Multiferroic $LuFe_2O_4$

J.L. Musfeldt, X.S. Xu, T.V. Brinzari (UT, Chemistry), S. McGill (Magnet Lab), M. Angst, R. Hermann (Julich, Physics), A.D. Christianson, D. Mandrus (ORNL), J.-W. Kim (Ames), Z. Islam (Argonne)

INTRODUCTION

Complex oxides take advantage of the unique and flexible properties of transition metal centers to govern bonding and local structure. Further, the delicate interplay between charge, structure and magnetism yields important consequences for functionality and cross-coupling. Iron-based materials such as multiferroic $BiFeO_3$ and $LuFe_2O_4$ have attracted recent attention. In this work, we focus on $LuFe_2O_4$, a frustrated system with a series of phase transitions that gives rise to electronically driven multiferroicity.
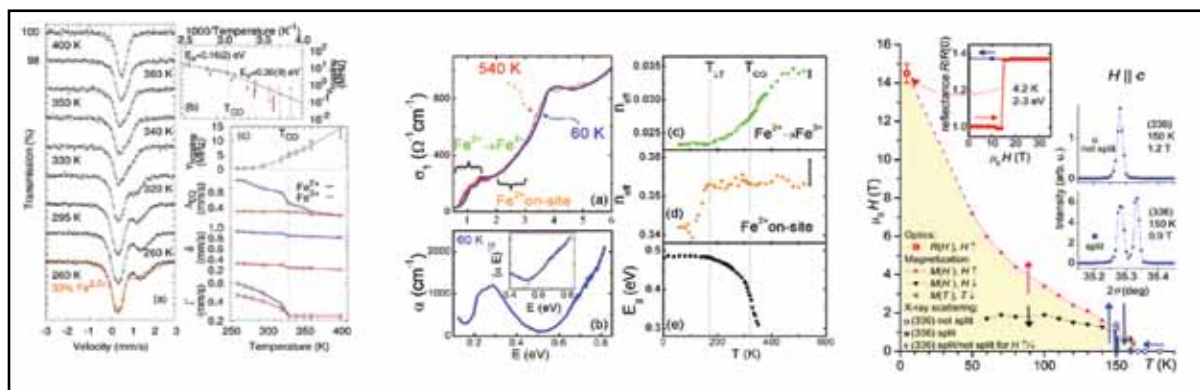

Figure 1.
Optical properties of $LuFe_2O_4$ and H-T phase diagram generated from combined optical, magnetic, and structural studies. **a:** σ_1 vs energy E at 540 and 60 K calculated from a Kramers-Kronig analysis of reflectance. Brackets indicate assignment from electronic structure calculations. **b:** α vs E calculated from transmittance, showing the charge transfer edge starting from ~0.5 eV. **c, d:** $n_{eff}(T)$ calculated by the partial sum rule for Fe^{2+} to Fe^{3+} charge transfer and Fe^{2+} on-site excitations. **e:** $E_g(T)$ calculated from an absorption edge fit assuming an indirect gap. Combined magnetization, structural and optical measurements allow us to generate an H-T phase diagram.

RESULTS AND DISCUSSION

To elucidate the charge excitations and understand how they correlate with structure and magnetism, we measured the optical and Mossbauer spectra, magnetization and x-ray scattering of $LuFe_2O_4$. We compare our comprehensive results to recent electronic structure calculations and to spectral data on classical magnetite. We demonstrate that strong Fe^{2+} to Fe^{3+} charge fluctuation persists even in charge ordered states characterized by superstructure reflections, and it persists down to T_{LT} below which Bragg splitting indicates that strong monoclinic distortions occur. These observations are consistent with the "order by fluctuation" mechanism, in which case $\sqrt{3} \times \sqrt{3}$ charge order is preferable for entropy reasons and stabilized by the charge fluctuation in this geometrically frustrated system. As in magnetite, we analyze the results in terms of a polaron picture, extracting a large effective mass for the charge carriers. On the other hand, Fe^{2+} on-site excitations are sensitive to the magnetic transition at 170 K and display a sizable magneto-optical effect. Combining our spectral, magnetic, and structural data, we generate an H-T phase diagram and show that the low temperature transition can also be driven by a magnetic field. These results demonstrate the important interplay between charge, structure and magnetism.

ACKNOWLEDGEMENTS

This study in the 50 tesla (T) mid-pulse magnet at Los Alamos and the 45 T hybrid magnet in Tallahassee involves magnetic and thermal measurements of dimerized (paired) spin-1 Mn^V ions arranged on a triangular lattice. Application of a field favors parallel spin alignments, whereas the intrinsic interaction between dimers that strives for antiparallel neighboring spins is frustrated because of the triangular topology. This competition forces the spins into adopting a rich variety of unusual spiral ordered phases.

Multiple Magnetic Phases in the Frustrated S=1 Spin-Dimer Compound $Ba_3Mn_2O_8$

E.C. Samulon M. C. Shapiro, I. R. Fisher (Stanford University, Applied Physics); R. D. McDonald, Y. Kohama, M. Jaime (Magnet Lab, LANL); K.A. Al-Hassanieh, C.D. Batista (Theoretical Division, LANL)

INTRODUCTION

Spin dimer compounds comprise pairs of strongly coupled magnetic ions. Antiferromagnetic intradimer exchange leads to a ground state that is a product of singlets, but an applied magnetic field can be used to close the spin gap to excited triplet states [Figure 1(a)], resulting at low temperatures in a state characterized by long range magnetic order. Under favorable conditions a variety of interesting magnetic states can be realized, including a Bose-Einstein condensate[1] and possibly even a spin supersolid[2].

$Ba_3Mn_2O_8$ is a spin dimer compound based on vertical pairs of S=1 $3d^2$ Mn^{5+} ions arranged on a triangular lattice. Previous measurements performed at the Magnet Lab revealed multiple ordered states where the triplet state crosses the singlet state[3]. Our more recent experiments at the Magnet Lab revealed an additional ordered state as the gap to the quintuplet states is closed. Substantial asymmetry in this quintuplet condensate can be related to the presence (absence) of phase fluctuations at the lower (upper) critical field in the quintuplet condensate.
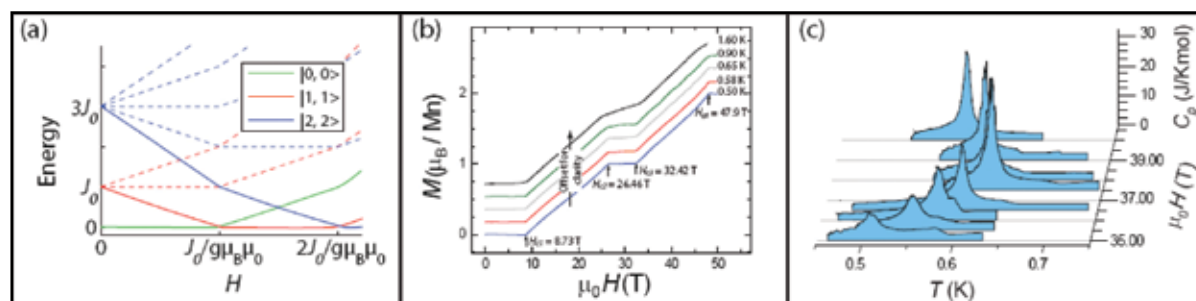

Figure 1.

(a) Energy level diagram from isolated dimer with antiferromagnetic intradimer exchange J_0. (b) Magnetization curves taken at successive temperatures. Positions of critical fields determined from second derivative with respect to field. (c) Heat capacity curves, taken on cooling for fields perpendicular to the dimer axis, as a function of temperature and field showing transitions into the triplet-quintuplet ordered state.

EXPERIMENT AND RESULTS

Magnetization measurements were performed at temperatures down to 0.5 K in the 50 T mid-pulse magnet at the Magnet Lab in Los Alamos. These measurements revealed two different regimes of linearly increasing magnetization as the triplet and quintuplet bands are filled [Figure 1 (b)]. Heat capacity and magnetocaloric effect experiments were also undertaken in the hybrid magnet at the Magnet Lab in Tallahassee at temperatures down to 0.5 K [Figure 1(c)]. Those experiments revealed a third distinct ordered state in the phase diagram for $Ba_3Mn_2O_8$ above 33 T where the quintuplet band crosses the triplet band.

DISCUSSION

The remarkable phase diagram of $Ba_3Mn_2O_8$ (Figure 2) contains at least three ordered states across the triplet and quintuplet regimes. Analysis of the minimal spin Hamiltonian describing this system indicates that each of the phases are novel modulated spiral structures characterized by multiple order parameters, arising as a consequence of the competition between the effects of interdimer coupling on a triangular lattice and single ion anisotropy[3]. In addition, inspection of Figure 2 reveals a substantial asymmetry in the quintuplet condensate not present in the triplet condensate. This effect is a consequence of zero-point phase fluctuations, present at H_{c1}, H_{c2} and H_{c3} but absent at H_{c4}.
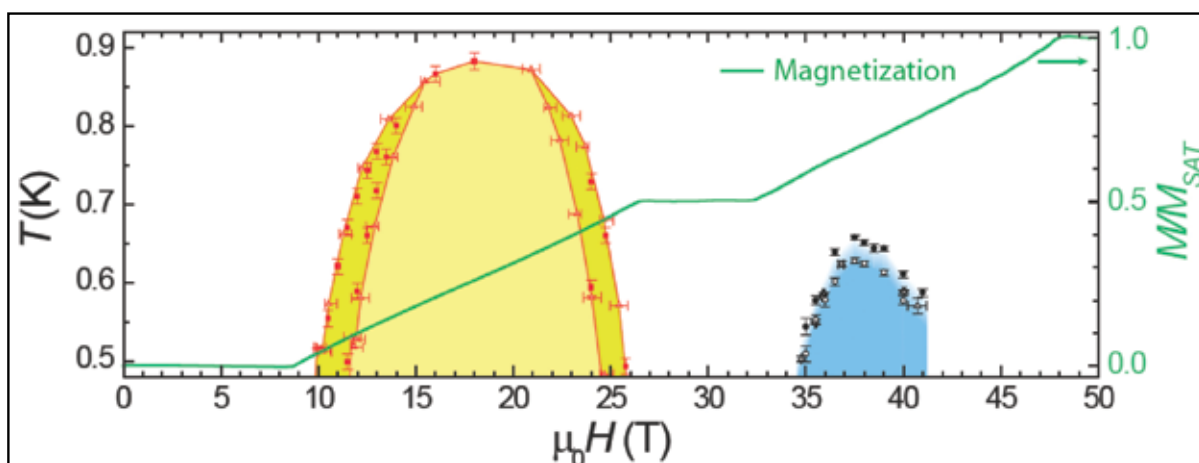
CONDENSED MATTER PHYSICS

Figure 2.
Phase diagram obtained from heat capacity (circles) and MCE (triangles) measurements for fields perpendicular to the dimer axis. Yellow and blue regions correspond to singlet/triplet and triplet/quintuplet ordered states, respectively. Magnetization curve taken at 0.50 K plotted along right axis.

ACKNOWLEDGEMENT

REFERENCES

1. S.E. Sebastian *et al.*, *Nature,* 441, 617 (2006).
2. P. Sengupta *et al.*, *Physical Review Letters,* 98, 227201 (2007).
3. E.C. Samulon *et al.*, *Physical Review B*, 77, 214441 (2008).

A long standing problem in condensed matter physics concerns the properties of spin-1/2 particles on a triangular lattice when the interactions between adjacent spins favors anti-alignment. Because of the geometric frustration (impossibility to satisfy all pairwise interactions) inherent in such situations, quantum mechanical effects end up dominating the low-temperature magnetism. Fortune *et al.* (including undergraduate student Adrienne Wilson-Muenchow) report sensitive low-temperature thermal measurements on Cs_2CuBr_4, which reveal an unexpected cascade of high-field ordered phases, suggesting that quantum effects continue to dominate to fields that are much higher than previously predicted. This research activity is an example of Magnet Lab user programs providing opportunities to faculty and students at undergraduate institutions.

This work has been submitted to *Physical Review Letters*

• This research was supported by the Magnet Lab's User Collaboration Grants Program.

Cascade of Magnetic-Field-Induced Quantum Phase Transitions in the S=1/2 Triangular-Lattice Antiferromagnet Cs_2CuBr_4

N.A. Fortune, A. A. Wilson-Muenchow (Smith College, Physics); S.T. Hannahs (Magnet Lab, FSU); Y. Yoshida, Y. Takano (UF, Physics); T. Ono, H. Tanaka (Tokyo Inst. Tech., Physics)

INTRODUCTION

In a geometrically frustrated spin-1/2 Heisenberg antiferromagnet on a triangular lattice, spin-wave theory[1] predicts that the lifting of the classical degeneracy by quantum fluctuations will lead to the appearance of a collinear up-up-down phase at 1/3 of the saturation magnetization M_s[1], as observed in Cs_2CuBr_4 [2]. We have extended the high-magnetic-field phase diagram of this material to the saturation field H_s =28.5 tesla (T) for fields directed along the crystallographic *c* axis using the magnetocaloric effect as a probe, and in so doing, have discovered an unexpected series of additional gapped collinear spin states bounded by first order transitions at simple increasing fractions of the saturation magnetization.

EXPERIMENTAL

The experiment was performed in the 50-mm diameter bore, 31 T magnet at the Magnet Lab DC Field Facility. A single-crystal sample of Cs_2CuBr_4 was placed in a miniature calorimeter[3] housed in a small plastic vacuum capsule that is top-loaded into the mixing chamber of a dilution refrigerator. To better detect the small-size features associated with some of the transitions, we minimized the addenda of the calorimeter by directly mounting the sample on a small 50 μm thin ruthenium-oxide thermometer and stabilized the

temperature of the thermal reservoir (to which the sample-thermometer combination is weakly coupled) by continuously updating the set point of the temperature regulator as the magnetic field was varied.

RESULTS AND DISCUSSION

The phase diagram constructed from this work (and our previous measurements below 18 T) is shown in the figure above. The antiferromagnetically ordered phases labeled 1/3, B, and 2/3 are believed to be commensurate and collinear; the phases labeled with Roman numerals I through V are either known to be or likely to be incommensurate. Magnetization data[4] suggests that the B and '2/3' phases form magnetization plateaus at 5/9 and 2/3 of the saturation magnetization M_s. Supporting evidence for the commensurate nature of the very narrow B phase comes from NMR[5]. The A phase occurs where the magnetization is close to ½ of the saturation value M_s, although it does not form a magnetization plateau. Surprisingly, all three phases with magnetization plateaus — including the 1/3 phase — are bounded by first-order transition lines.

High-field phase diagram of Cs_2CuBr_4 with magnetic field along the c axis.

ACKNOWLEDGEMENTS

REFERENCES
1. A.V. Chubukov *et al.*, *J. Phys.: Condens. Matter*, **3**, 69–82 (1991).
2. T. Ono *et al.*, Phys. Rev. B, **67**, 104431 (2003).
3. S.T. Hannahs *et al.*, *Physica B*, **329–333**, 1586–1587 (2003).
4. T. Ono *et al.*, *J. Phys.: Condens. Matter*, **16**, S773–S778 (2004).
5. Y. Fujii *et al.*, unpublished.

Numerous experiments on two-dimensional (2D) electron and hole systems in semiconductor heterostructures have produced strong evidence in favor of the existence of a metal-insulator transition (MIT) in 2D, one of the fundamental, but poorly understood, problems in condensed matter physics. Much of the experimental work has been performed at the Magnet Lab. Now, a theoretical group at the Magnet Lab, led by V. Dobrosavljević, and collaborators at Rutgers, report on a scenario of quantum melting of a Wigner crystal as the mechanism of the MIT in sufficiently clean samples. They show that, by ignoring disorder and focusing on interaction effects alone, the theory can reproduce many of the key experimental results, including the phase diagram in a magnetic field.

This is an excellent example of Mag Lab-affiliated theorists directing the great promise of dynamical mean-field theory to address problems of long-standing interest to high magnetic field experiments.

• This work was published in *Physical Review B*, **77**, 085104 (2008) and *Nature Physics* **4**, 932 (2008).

2D-MIT as a Wigner-Mott Transition

S. Pankov and V. Dobrosavljević (Magnet Lab); A. Camjayi, K. Haule, and G. Kotliar (Rutgers University)

INTRODUCTION

Significant experimental advances (1) over the last 10 years have provided beautiful and convincing evidence for the existence of a sharp metal-insulator transition (MIT) in two-dimensional (2D) electron gases (2DEG). This progress has sparked much renewed interest in better understanding the basic physical mechanisms that drive the MIT, a fundamental physical question that has remained poorly understood for many years. It should be emphasized, though, that the best evidence for a sharp MIT is found in the cleanest samples, where the diffusive regime is restricted to low densities and extremely low temperatures. Indeed, the experimental data[1] demonstrating strong effective mass m* enhancements have all been obtained in the ballistic regime, where diffusive processes are irrelevant. An important question then arises: How many of the key experimental features can be understood by deliberately disregarding disorder, and focusing on

CONDENSED MATTER PHYSICS
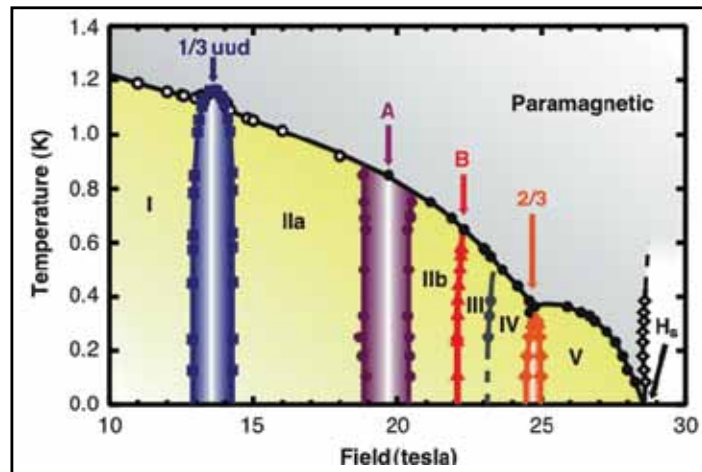
CONDENSED MATTER PHYSICS

interaction effects alone as the main driving force for the transition? This question is the main subject of the work presented in Ref. 2, where we propose the quantum melting of a Wigner crystal as the fundamental mechanism for the MIT in a sufficiently clean 2DEG. Here, we presented a simplified description of a Wigner crystal, based on the idea that there exists a pronounced short range order in charge sector both on the metallic and insulating sides of the MIT. While this theory reproduced many aspects of the experiment, a more accurate description should explicitly include the dynamics of collective charge fluctuations, which were phenomenologically treated in Ref. 2. A more comprehensive theory describing both the charge ordering and the metal-insulator transition, which provides further support to the results of Ref. 2, has been presented in Ref. 3.

RESULTS AND DISCUSSION

In Ref. 3, we show that strong correlations, normally expected only for narrow integer filled bands, can be effectively enhanced even far away from integer filling, due to incipient charge ordering driven by non-local Coulomb interactions. This general mechanism is illustrated by solving an extended Hubbard model using dynamical mean-field theory. Our findings account for the key aspects of the experimental phase diagram, and reconcile the early viewpoints of Wigner and Mott. The interplay of short range charge order and local correlations should result in a three peak structure in the electron spectral function, which can be observed in tunnelling and optical spectroscopy. These experiments will discriminate between the Wigner-Mott scenario and the alternative perspective that views disorder as the main driving force for the 2D-MIT.

CONCLUSIONS

We presented the solution of a simple microscopic model that correctly captures the qualitative behavior near a Mott transition in the presence of a charge ordered background (Wigner-Mott transition). As in the conventional Mott scenario, this transition features the formation of a strongly correlated state on the metallic side. The magnetic field dependence proves to be dramatically different from what is expected in a one band Hubbard model at half filling but it is in favorable agreement with experiments on the 2DEG.

ACKNOWLEDGEMENTS

REFERENCES
1. S. V. Kravchenko and M. P. Sarachik, *Rep. Prog. Phys.*, **67**, 1 (2004)
2. S. Pankov and V. Dobrosavljević, *Phys. Rev. B*, **77**, 085104 (2008).
3. A. Camjayi *et al.*, *Nature Phys.*, **4**, 932 (2008).

A hallmark of strong correlation effects in high-quality, dilute, two-dimensional (2D) electron systems is a marked increase in the effective mass (m*) of electrons as the density is lowered and the system is made more interacting. This report describes measurements on 2D electrons in an AlAs quantum well that reveal variations of m* with spin and valley polarizations. They find that, although m* is enhanced compared to the band value (mb) in the partially spin and/or valley polarized cases, when the 2D system is fully spin- and valley-polarized, m* is suppressed down to values near or below mb. These results reveal that, besides diluteness, the discrete electronic degrees of freedom, such as spin and valley, play an essential role in determining fundamental properties of an interacting system.

• This work was published in *Physical Review Letters*, **101**, 146405 (2008).

Dependence of Effective Mass on Spin and Valley Degrees of Freedom

T. Gokmen, Medini Padmanabhan, M. Shayegan (Princeton University)

INTRODUCTION

Electron-electron interaction renormalizes the effective mass (m*) of carriers confined to two dimensional (2D) systems. Therefore m* is a fundamental quantity of interest to probe interaction effects in 2D systems. We studied the role of the spin and valley degrees of freedom on m*. We found that, although m* is enhanced compared to the band value (m_b) in the partially spin and/or valley polarized cases, when the 2D system is fully spin- and valley- polarized, m* is suppressed down to values near or below m_b.

EXPERIMENTAL

We performed magnetotransport measurements on a 2D electron system confined to an 11 nm-wide

AlAs quantum well at a fixed density while we changed the conduction band valley occupation and spin polarization via the application of strain and magnetic field, respectively. Measurements were done in the 18/20 T DC magnet of the Magnet Lab millikelvin facility using standard low-frequency lock in techniques at temperatures from 20 mK to 1 K. The sample was mounted on a tilting stage that enabled us to apply high parallel magnetic fields necessary for complete spin polarization.

RESULTS AND DISCUSSION

We measured m^* via analyzing the temperature dependence of the Shubnikov-de Haas oscillations at a density of $n = 3.8 \times 10^{11}$ cm^{-2}. Figures 1 (a) and (b) show the sample resistance as a function of parallel magnetic field or strain, respectively. We used these traces to determine the spin/valley polarization of the sample. Figure 1 (c) shows the four possible spin and valley occupations in a parallel field vs. strain "phase diagram." The stars show the coordinates where we measured m^* in these four quadrants, and the deduced m^* values are indicated next to the stars. Our results provide direct experimental evidence for the dependence of m^* on valley and spin polarization of the 2D system.

Figure 1.

CONCLUSION

In summary, we observed that the effective mass of electrons confined to a quantum well in AlAs is greatly influenced by the spin and valley degrees of freedom. Mass is suppressed only when the system is fully spin and valley polarized; otherwise m^* is enhanced above m_b.

ACKNOWLEDGEMENTS

REFERENCES

1. Medini Padmanabhan *et al.*, *Phys. Rev. Lett.*, **101**, 026402 (2008).
2. T. Gokmen *et al.*, *Phys. Rev. Lett.,* **101**, 146405 (2008).
3. T. Gokmen *et al.*, *Phys. Rev. B.,* **78**, 233306 (2008).

Dilute two-dimensional (2D) electron systems subject to strong perpendicular magnetic fields find themselves in highly correlated states that emerge as a result of the interplay between electron–electron interactions, confinement and disorder. These states ultimately give way to a periodic electron solid (2D Wigner crystal) that crystallizes at high magnetic fields. This report describes the discovery of a new insulating quantum phase of electrons when, in addition to a perpendicular field, a very high magnetic field is applied in a geometry parallel to the 2D electron sheet. The data point toward this new quantum phase being an electron solid in a "quasi-3D" configuration induced by orbital coupling with the parallel field.

• This work was published in *Nature Physics*, **4**, 936 (2008).

Wigner Crystallization in a Quasi-Three-Dimensional Electron System

B.A. Piot (McGill, Physics), Z. Jiang (Magnet Lab, Columbia), C.R. Dean (McGill, Physics), L.W. Engel (Magnet Lab), G. Gervais (McGill, Physics), L.N. Pfeiffer (Alcatel-Lucent, Bell Labs) and K.W. West (Alcatel-Lucent, Bell Labs)

INTRODUCTION

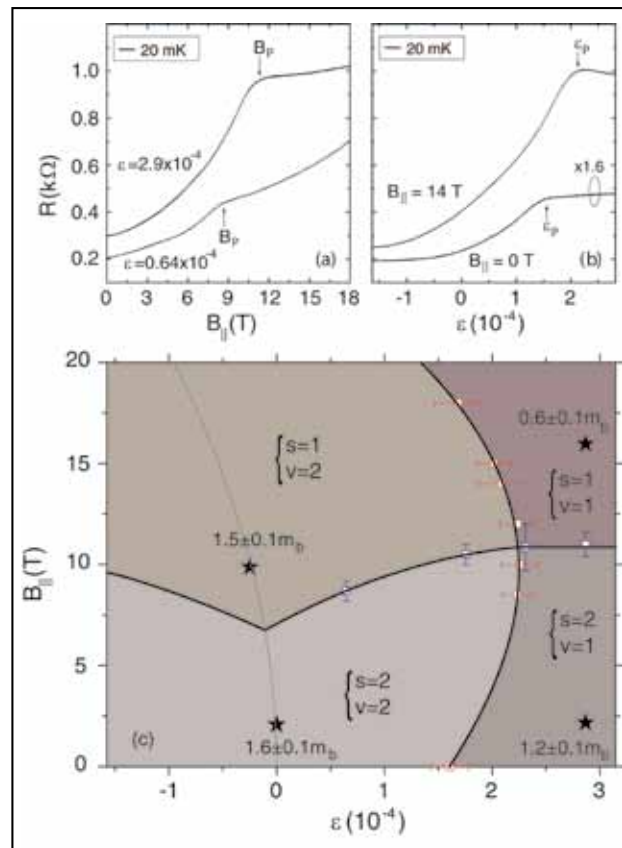When a strong magnetic field is applied perpendicularly (along z) to a sheet confining electrons to two

CONDENSED MATTER PHYSICS

CONDENSED MATTER PHYSICS

dimensions (x-y), highly correlated states emerge as a result of the interplay between electron-electron interactions, confinement and disorder. These so-called fractional quantum Hall (FQH) liquids form a complete series of states that ultimately give way to a periodic electron solid that crystallizes at high magnetic fields. Here, we report[1] our discovery of a new insulating quantum phase of electrons when a very high magnetic field, up to 45 tesla (T), is applied in a geometry parallel (y-direction) to the two-dimensional electron sheet. Our data point towards this new quantum phase to be a quasi-3D electron solid induced by orbital coupling with the parallel field.

Figure 1.

EXPERIMENTAL

The 2DEGs studied here are 40 nm wide modulation-doped GaAs quantum wells, all from the same wafer grown by molecular beam epitaxy. The samples were cooled in a dilution fridge with base temperature T~35 mK installed inside a hybrid superconducting/resistive magnet capable of reaching a total magnetic field of 45 T.

RESULTS AND DISCUSSION

We show a phase diagram for the insulator at high tilt (parallel field) in Figure 1. The smooth crossover between the low-theta and high-theta regions of the phase diagram is strong evidence for a continuous evolution between a perpendicular-field dominated 2D Wigner crystal and a electron solid stabilized in a "quasi-3D" system. The right panel of Figure 1 also shows a scatter plot for the values obtained for the "parallel filling factor" at the onset of the insulating phase. Strikingly, the transitions from a FQH liquid to an insulating phase in this regime all occur very closely to an average parallel filling factor of 0.22, shown by a dashed vertical line. These critical parallel filling factors are remarkably similar to those associated with the onset of the conventional 2D x-y Wigner crystal. This striking similarity between
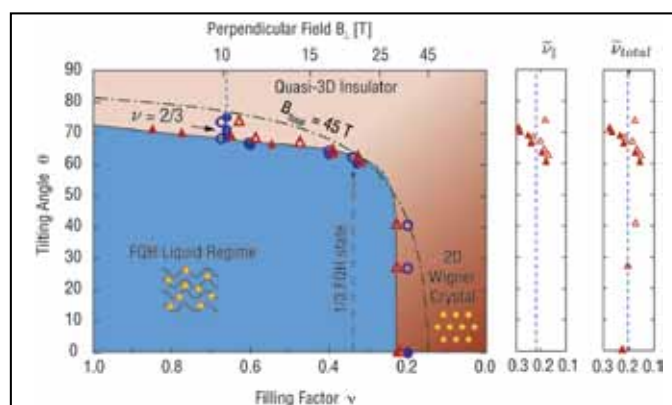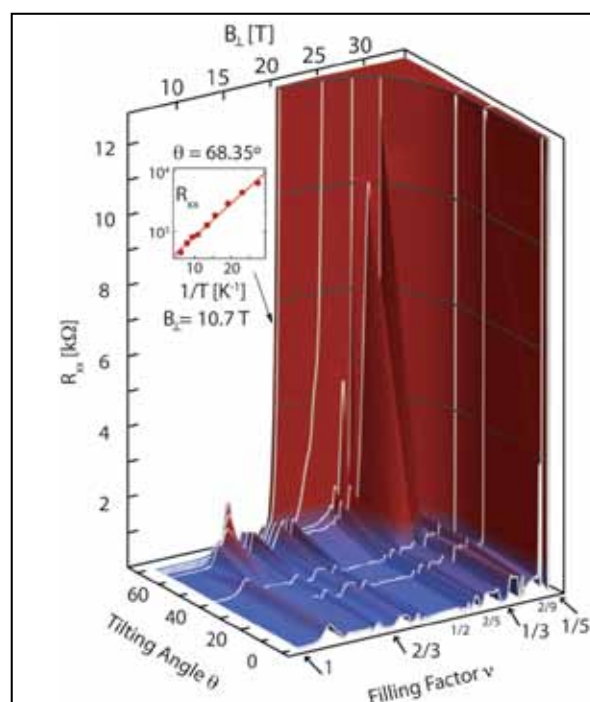

Figure 2.
The resistance of sample C as a function of the perpendicular magnetic field $B_\perp$ (or equivalently the filling factor ν) for different tilting angles θ and T≈35 mK. White lines are actual data, and the trend in between is extrapolated as a guide to the eye. The resistance value is emphasized by a colour map, with the black lines corresponding to equi-resistance. Inset: Temperature dependence of R_{xx} at $\theta = 68.35°$ and $B_\perp = 10.7$T.

the x-y and z-x configurations point toward the formation of an electron solid in the z-x plane owing to a simple reduction in occupation in its first magnetic level and crystallization. This solid occurs for the parallel magnetic length sufficiently small relative to the quantum well width, so that electrons acquire the freedom to minimize their mutual repulsion by adjusting their positions in the z-direction.

CONCLUSIONS

In conclusion, we have observed a new electronic insulating quantum phase at filling factors higher than 1/5 when tilting a 2DEG in a very high magnetic field, up to 45 T. We have shown that electrons in this phase become orbitally coupled to the parallel field and transition from electric to magnetic confinement. We interpret this new phase as an evolved Wigner crystal with distorted broken symmetry along the z-x plane.

ACKNOWLEDGEMENTS

REFERENCES
1. B.A. Piot *et al.*, *Nature Phys.*, **4**, 936 (2008).

CONDENSED MATTER PHYSICS

Even-denominator fractional quantum Hall (FQH) states are of potential relevance to topological quantum computing schemes, but observations of such states have been rare. This report describes the observation of a FQH state at ν=1/4 in a wide quantum well. However, the origin of this state is yet to be determined.

• This work was published in *Physical Review Letters*, **101**, 266804 (2008).

Evidence for a Fractional Quantum Hall State at ν =1/4 in a Wide Quantum Well

D.R. Luhman (Princeton University), W. Pan (Sandia National Laboratories) D.C. Tsui (Princeton University), L.N. Pfeiffer (Bell Labs), K.W. Baldwin (Bell Labs), and K.W. West (Bell Labs)

INTRODUCTION

Interest in the even-denominator fractional quantum Hall (FQH) state at ν=5/2 continues to remain high, partially due to its potential relevance in fault-tolerant, topological quantum computing schemes. Yet observations of even-denominator FQH states have been rare beyond the ν=5/2 state in single-layer systems. In particular, there is no evidence of a FQH state at ν=1/2. In bilayer systems the situation is different. The presence of two nearby, interacting electron layers introduces an additional degree of freedom that can give rise to the formation of a FQH state at ν=1/2, which, indeed, has been observed in double quantum wells[1] and in wide single quantum wells (WSQWs)[2]. In general a similar state should also occur at ν=1/4, however, to the best of our knowledge it has not been observed experimentally. An observation of a FQHE state at ν=1/4 would not only be important in itself but also may shed more light on the origin of still enigmatic ν=1/2 FQH state in WSQWs.

EXPERIMENTAL

To search for a FQH state at ν=1/4 we have used a high-quality GaAs quantum well with a well width of 50 nm, an electron density of $n = 2.55 \times 10^{11}$ cm^{-2}, and a mobility of 10^7 cm^2/Vs. We have measured the electronic transport properties of this sample at $T \sim 35$ mK in magnetic fields up to 45 tesla (T) using the Hybrid facility at the Magnet Lab.

RESULTS AND DISCUSSIONS

As shown in Figure 1, when the sample is perpendicular to the magnetic field, the diagonal resistance displays a kink and the Hall resistance shows a subtle deviation from the classical slope at ν=1/4. When the sample is tilted to an angle θ =20.3°, the kink develops into a strong R_{xx} minimum and a plateau emerges in R_{xy}, clearly demonstrating a FQH state at ν=1/4. As to the origin of

Figure 1.
R_{xx} and R_{xy} as a function of the perpendicular component of magnetic field, B_{perp}, for θ=0° and 20.3° at $T \sim 35$ mK.

the ν = 1/4 state, one possibility is a two-component Halperin state such as {553} or {771}. On the other hand, the possibility that ν = 1/4 state is described by {771} is unlikely considering the bilayer interpretation of the {nnm} wavefunctions. For the {771} wavefunction the electron filling factor in each layer would be ν = 1/7 and typical single-layer two-dimensional electron systems (2DESs) enter into an insulating phase beyond ν = 1/5 at low temperatures. An alternate possible description for the observed ν = 1/4 state may be the pairing of composite fermions, similar to the proposal for a ν = 1/2 FQH state in a thick 2DES[3].

CONCLUSIONS

Our data provide evidence for the existence of a FQH state at ν=1/4 in our sample. The origin of this state has yet to be determined.

REFERENCES
1. J.P. Eisenstein *et al.*, *Phys. Rev. Lett.*, **68**, 1383 (1992).
2. Y.W. Suen *et al.*, *Phys. Rev. Lett.*, **68**, 1379 (1992).
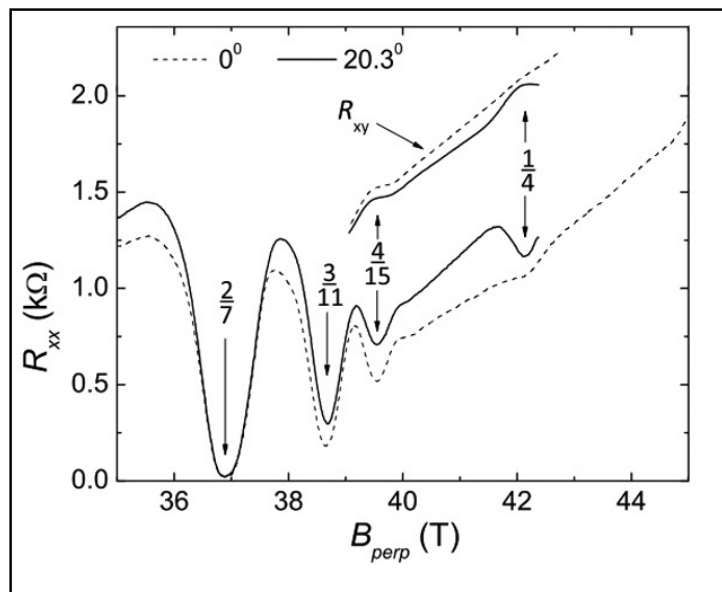3. K. Park *et. al.*, *Phys. Rev. B*, **58**, R10167 (1998).

CONDENSED MATTER PHYSICS

In bismuth, when **H** is nearly aligned with the trigonal axis **Z**, the projected area of the hole Fermi surface is nearly equal to that of each electron ellipsoid preventing the electron Landau Levels (LL) from being observed. Using high-resolution torque magnetometry, and **H** at a small tilt angle, the electron signals are greatly amplified enabling separation of the electron and hole Fermi surfaces. At higher fields, jumps in the magnetization were observed and attributed to a many-body state in which the 3-fold valley degeneracy of the Dirac electrons is lifted.

• This work was published in *Science*, **321**, 547 (2008).

Phase Transitions of Dirac Electrons in Bismuth

Lu Li, J. G. Checkelsky, and N. P. Ong (Princeton Univ.)

INTRODUCTION

In the semi-metal element bismuth, the Fermi surface (FS) is composed of three electron ellipsoids and one hole ellipsoid. The three electron FS have a linear energy-momentum dispersion well described by the Dirac Hamiltonian. A long-standing impediment to the investigation of the Dirac electrons in high magnetic fields **H** is that when **H** is nearly aligned with the trigonal axis **Z**, the projected area of the hole FS is nearly equal to that of each electron ellipsoid. This has prevented the electron Landau Levels (LL) from being observed. Using high-resolution torque magnetometry, we have shown that with **H** at a small tilt angle θ to **Z**, the electron signals are greatly amplified. This has allowed us to resolve the electron LLs from the holes. Extending the torque measurements to higher fields, we observe jumps in the magnetization that imply a field induced transition to an interesting many-body state in which the 3-fold valley degeneracy of the Dirac electrons is lifted.

RESULTS AND DISCUSSION

As shown in Figure 1, the field $B(n, \pm)$ at which the LL with indices $(n, \pm)$, where $\pm$ labels the Kramers doublet, crosses the chemical potential disperses strongly with tilt angle θ (consistent with electron FS as opposed to the hole FS). At fields above 9 tesla (T), we observe the emptying of the last-but-one LL (0,-).

Above 9 T, we observe a jump in magnetization at the field H_1, which signals a field-induced transition to the region shaded white. The right panel shows traces of the transverse magnetization M_{trans} vs. tilt angle θ in fixed field (9 < H < 31 T). The jump in M_{trans} as θ crosses the boundaries of the cone-shaped region is evident. We interpret the jumps as field-induced transitions to a many-body state in which the 3-fold valley degeneracy is lifted. Within the cone shaped region, the electrons occupy a linear combination of valley states with much lower exchange energy.
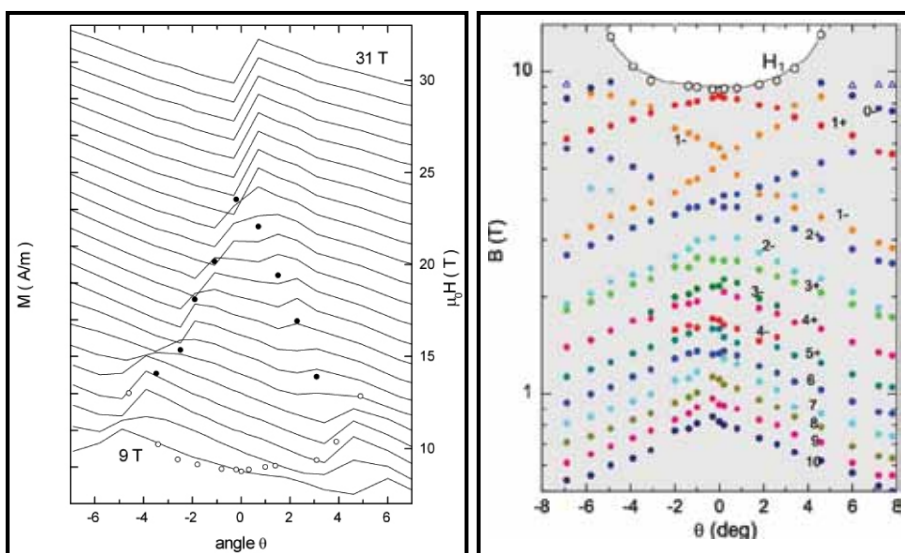

Figure 1.

Left panel shows the fields $B(n, \pm)$ at which Landau sub-level $(n, \pm)$ in bismuth cross the chemical potential ($\pm$ indexes the Kramers degeneracy). The crossings are inferred from torque magnetometry performed with **H** at a small tilt angle θ to the trigonal axis **Z**. The steep θ dependence of $B(n, \pm)$ reflects the strong LL dispersion in the Dirac electron pockets. The curve H_1 marks a transition to a many-body state above 10 tesla (T). The right panel plots the transverse magnetization M_{trans} vs. θ at selected field values from 9 to 31 T. The discontinuities at H_2 (solid circles) and at H_1 (open circles) define transitions to the many-body state. (For details see Li et al.[3]).

ACKNOWLEDGEMENTS

REFERENCES
The following papers acknowledge support from the Magnet Lab:

1. J. G. Checkelsky *et al., Phys. Rev. Lett.*, **100**, 206801 (2008).
2. J. G. Checkelsky *et al., Phys. Rev. B*, **77**, 014433 (2008).
3. Lu Li *et al., Science*, **321**, 547 (2008).
4. J.G. Checkelsky *et al.*, "Divergent resistance at the Dirac point in graphene: evidence for a transition in high magnetic field." Cond-mat arXiv:0808.0906v1.
5. J. G. Checkelsky *et al.*, "Large quasiparticle thermal Hall conductivity in the superconductor $Ba_{1-x}K_xFe_2As_2$." Cond-mat arXiv: 0811:4668v1.

MLR

For solid-state systems, coupling to a fluctuating spin bath is a major source of decoherence in spintronics and spin-based quantum information processing devices. One approach to reduce decoherence is to fully polarize the spin bath. This work investigated the relationship between the spin coherence of nitrogen-vacancy (N-V) centers in diamond and the polarization of the surrounding nitrogen (N) spin bath, the most promising solid-state spin system for room temperature quantum information processing devices. Using 240 GHz continuous wave and pulsed EPR spectrometers it was demonstrated that it is possible to polarize strongly the N spin bath and quench spin decoherence.

• This work was published in *Physical Review Letters*, **101** (4), 047601(2008).

Quenching Spin Decoherence in Diamond through Spin Bath Polarization

S. Takahashi (UCSB, Physics and Institute for Terahertz Science and Technology); R. Hanson (TU Delft, Kavli Institute of Nanoscience and UCSB, Center for Spintronics and Quantum Computation); J. van Tol (Magnet Lab, EMR); M. S. Sherwin (UCSB, Physics and Institute for Terahertz Science and Technology); and D. D. Awschalom (UCSB, Physics and Center for Spintronics and Quantum Computation)

INTRODUCTION

Overcoming spin decoherence is critical to spintronics and spin-based quantum information processing devices. For spins in the solid state, a coupling to a fluctuating spin bath is a major source of the decoherence. One approach is to bring the spin bath into a well-known quantum state that exhibits little or no fluctuations. A prime example is the case of a fully polarized spin bath. The spin bath fluctuations are fully eliminated when all spins are in the ground state. Here we investigate the relationship between the spin coherence of nitrogen-vacancy (N-V) centers in diamond and the polarization of the surrounding spin bath consisting of nitrogen (N) electron spins. The N-V center in diamond is the most promising solid-state spin system for room temperature quantum information processing devices.

EXPERIMENTAL

We employed 240 GHz continuous wave (cw) and pulsed EPR spectrometers in the EMR program at the Magnet Lab.

RESULTS AND DISCUSSION

The temperature dependence of spin decoherence time (T_2) for the N-V center is shown in Figure 1. Between room temperature and 20 K, we observed almost no temperature dependence with T_2. Below the Zeeman energy (11.5 K), T_2 increases drastically. By lowering the temperature further, T_2 increases up to 250 μs at 1.7 K and does not show noticeable increase below 1.7 K.

Figure 1.
Temperature dependence of spin decoherence time (T_2) for the N-V and N centers. Solid line shows the fit by the flip-flop model.

At high magnetic field, the fluctuations in the bath are mainly caused by energy-conserving flip-flop processes of the N spins. The spin flip-flop rate in the bath is proportional to the number of pairs with opposite spin and thus it strongly depends on the spin bath polarization. At 240 GHz and 2 K, the N spin bath polarization is 99.4%, which almost eliminates the spin flip-flop process. This experiment therefore verifies that the dominant decoherence mechanism of the N-V center in diamond is the spin-flop process of the N spin bath.
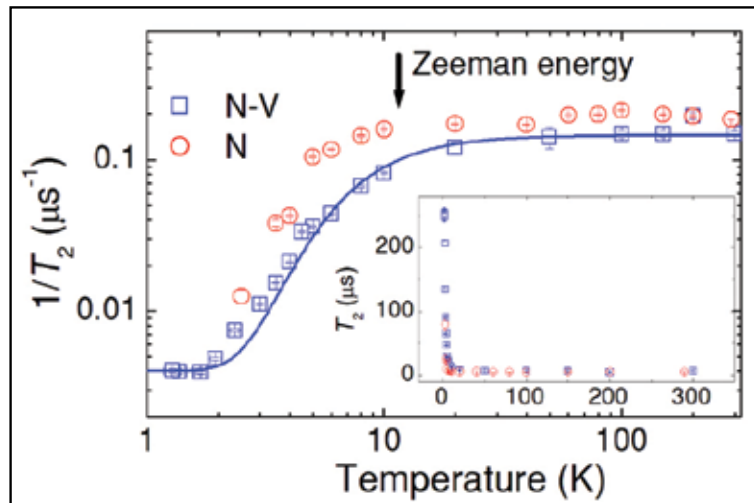
CONDENSED MATTER PHYSICS

As shown in Figure 1, agreement between the model and the T_2 data is excellent. Thus the result confirms the decoherence mechanism of the N spin bath fluctuation. Saturation of T_2 below 1.7 K proves that spin decoherence due to the N spin bath is quenched by complete polarization of the N spin bath. In addition, this saturation indicates that there exists a temperature-independent spin decoherence source.

CONCLUSIONS

We have demonstrated that we can strongly polarize the N spin bath and quench spin decoherence.

ACKNOWLEDGEMENTS

REFERENCES

1.   S. Takahashi *et al.*, *Phys. Rev. Lett.*, **101**, 047601 (2008).

Described here is the first observation of spin echoes from high-spin single-molecule magnet (SMM) single crystals. SMMs are nanoscale quantum magnets that exhibit quantum tunneling of magnetization and quantum phase interference. Because the molecules interact very weakly with each other, properties of a single molecule can be deduced from measurements of a macroscopic ensemble. Although quantum phenomena observed in SMMs have been investigated extensively, couplings between SMMs – important for applications to dense and efficient quantum memory, computing, and molecular spintronics devices – are still poorly understood, but can be studied via, for example, spin echoes.

This is a fine example where the unique high frequency EPR instrumentation developed at the Magnet Lab has enabled the study of spin relaxation processes in SMMs.

• This work was published in *Physical Review Letters*, **102** (8), 087603 (2009).

Coherent Manipulation and Decoherence of S=10 Single-Molecule Magnets

S. Takahashi (Physics and Institute for Terahertz Science and Technology); J. van Tol (Magnet Lab, EMR); C. C. Beedle, D. N. Hendrickson (UCSD, Chemistry and Biochemistry); L.-C. Brunel (Magnet Lab, EMR); and M. S. Sherwin (Physics and Institute for Terahertz Science and Technology)

INTRODUCTION

Single-molecule magnets (SMMs) are nanoscale quantum magnets that exhibit quantum tunneling of magnetization (QTM) and quantum phase interference (Berry phase). As solid-state based spin systems, SMMs form a unique class of materials that have a high-spin, and whose spin state and interaction can be easily tuned by changing peripheral organic ligands and solvate molecules. Because the molecules within the crystal lattice of SMMs interact very weakly with each other, properties of a single SMM can be deduced from measurements of a macroscopic ensemble. Although quantum phenomena observed in SMMs have been investigated extensively, couplings between SMMs and their environment are still poorly understood for proposed applications to dense and efficient quantum memory, computing and molecular spintronics devices.

EXPERIMENTAL

Spin relaxation times (T_1 and T_2) of S=10 Fe_8 SMM single crystals were investigated using 240 GHz continuous wave (cw) and pulsed EPR spectrometers at the Magnet Lab EMR facility.

RESULTS AND DISCUSSION

We observed spin echoes of the $m_S = -10 \leftrightarrow -9$ transition in S=10 Fe_8 SMM single crystals. This is the first observation of spin echoes from high-spin SMM single crystals.
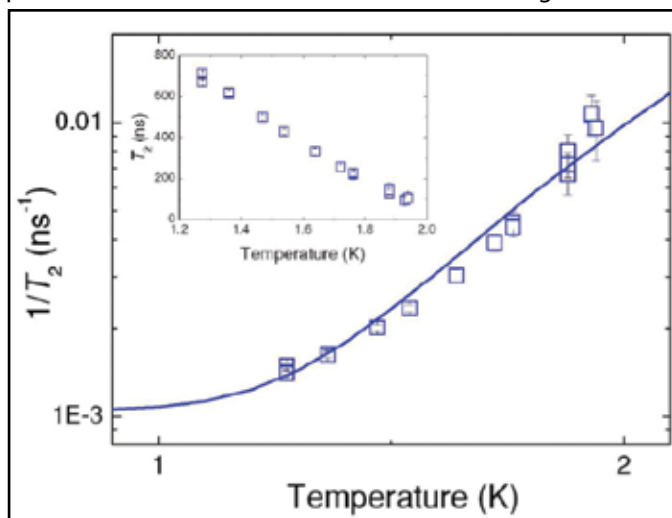

Figure 1.
Temperature dependence of T_2. Solid line shows the fit by the spin flip-flop model.

The spin-lattice relaxation time T_1 was directly measured at 1.3 K using a stimulated echo sequence. We found that stimulated echoes are detectable for more than a few milliseconds and that the echo decay curve shows two relaxation rates with a short time of $T_{short} = 1.0 \pm 0.1$ µs and a long time of $T_{long} = 948 \pm 108$ µs. Because of the small excitation bandwidth, a strong spectral diffusion is expected. Therefore we currently speculate that the T_{short} is due to spectral diffusion and the T_{long} is the spin-lattice relaxation time T_1. Surprisingly, this value of T_1 is more than two orders of magnitude longer than previous findings.

Figure 1 shows the temperature dependence of T_2. Observation of a strong temperature dependence of T_2 suggests that the main decoherence mechanism at higher temperatures is due to coupling to fluctuating neighboring electron spins, which is often pictured as a spin bath[1]. Since the cw EPR spectra show that Fe_8 SMMs dominate the population of electron spins in the sample crystal, the source of the Fe_8 spin decoherence is fluctuations of the Fe_8 spin bath itself. T_2 below 1 K is limited by other temperature-independent decoherence sources which are likely nuclear moments and phonons.

CONCLUSIONS

We demonstrated the first direct determination of T_1 and T_2 for Fe_8 SMMs single crystals using spin echoes. Spin decoherence is significantly suppressed by polarizing the Fe_8 spin bath. See Ref. 2 for details.

ACKNOWLEDGEMENTS

REFERENCES
1. S. Takahashi *et al.*, *Phys. Rev. Lett.*, **101**, 047601 (2008).
2. S. Takahashi et al., *Phys. Rev. Lett.,* **102** (8), 087603 (2009).

The idea of Bose-Einstein condensation (BEC) occurring in the spin systems of certain quantum magnets with axial symmetry has been explored extensively in the past few years. In those systems, the axial symmetry of the spins is expected to allow XY antiferromagnetic (AF) order to occur over certain ranges of temperature and magnetic field. The field-induced quantum phase transition at the boundary of the long-range ordered state can be modeled as a BEC. Here the authors report on the field-induced BEC in an organic compound by demonstrating the 3/2 power-law exponent in the temperature dependence of the critical field line, as expected for the 3D BEC universality class. This is the first example of a direct measurement of this exponent at temperatures (down to 1 mK) far below the energy scales for AF coupling in a magnetic insulator, and the lowest temperature ever used to investigate BEC in a quantum magnet.

• This work was published in *Physical Review Letters*, **101**, 187205 (2008).

Magnetic Susceptibility Measurements to 1 mK and 13 T to Determine the Universality Class of Bose-Einstein Condensation in Ni-Cl$_2$-4SC(NH$_2$)$_2$

V.S. Zapf (LANL-Magnet Lab), L. Yin (UF-Magnet Lab), J.S. Xia (UF-Magnet Lab), A. Padhuan-Filho (Instituto de Fisica, Universidade de Sao-Paulo), N.S. Sullivan (UF-Magnet Lab)

INTRODUCTION

Experimental studies are reported for measurements of the lower and upper critical fields, H_{c1} and H_{c2}, respectively, for the field-induced Bose-Einstein condensation in the organic compound $NiCl_2$-4SC(NH$_2$)$_2$. The transitions were determined from measurements of the AC magnetic susceptibility for temperatures down to 1 mK and for fields from 1 to 13 tesla (T). The key parameter is the exponent for the temperature dependence of H_{c1} given by $H_{c1}(T)-H_{c1}(0) = aT^\alpha$ which is predicted to be 3/2 for a 3D BEC condensation.

EXPERIMENTAL

High sensitivity measurements of the magnetic susceptibility of the organic magnet Ni-Cl$_2$-4SC(NH$_2$)$_2$ (or DTN) were used to determine the critical magnetic fields for transitions to the anti-ferromagnetic state. DTN contains two Ni^{2+} atoms that form two interpenetrating tetragonal lattices. At zero field, a uniaxial anisotropy splits the Ni S=1 triplet into a $S_z = 0$ ground state and a $S_z = \pm 1$ excited state. The $S_z = 1$ state is suppressed by an applied magnetic field parallel to the tetragonal c-axis via the Zeeman effect, thereby producing a magnetic ground state above 2 T. Anti-ferromagnetic coupling between the Ni atoms with exchange J_c=1.8K along the c-axis, and J_a=0.18 K perpendicular to the c-axis, produces long range order[1].

CONDENSED MATTER PHYSICS

RESULTS AND DISCUSSION

The temperature dependence of the upper and lower critical fields, H_{c2} and H_{c1} are shown in Figure 1 for a field sweep rate of 0.0068 T/min. The dashed circle shows an abnormal change in slope for H_{c2} at 160 mK. The dashed line is a fit to the equation $H_{c1}(T) - H_{c1}(0) \sim T^\alpha$ with $\alpha = 1.47 \pm 0.1$. For further details, see Ref. 2.

CONCLUSIONS

The results of experiments at ultra-low temperatures have established that the field-induced quantum phase transitions at H_{c1} in DTN belong to the 3D BEC universality class. This is the first example of a direct measurement of the power law exponent for the critical field at temperatures well below the energy scales for anti-ferromagnetic coupling in a magnetic insulator.

ACKNOWLEDGEMENTS

REFERENCES

1. T. Giamarchi *et al., Nature Physics*, **4**, 198 (2008).
2. L. Yin *et al., Phys. Rev. Lett.*, **101**, 187205 (2008).
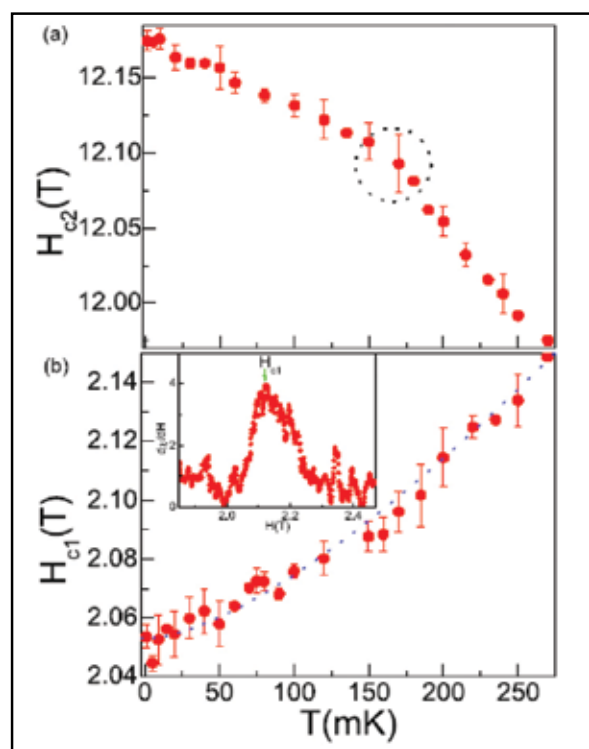
Figure 1.

Temperature dependence of (a) the upper critical field H_{c2}, and (b) the lower critical field H_{c1} for DTN. The points were obtained from measurements of the AC magnetic susceptibility down to 1 mK and for fields up to 13 T.

High magnetic fields enable exploration of otherwise inaccessible regions of the phase diagram of new categories of liquid crystals, and so are an important tool in furthering our understanding of what mesogenic states of matter are possible. This work confirmed a magnetic-field-induced first order phase transition in a bent-core liquid crystal, and achieved the first-ever observation of the loss of field-induced optical birefringence in a lyotropic chromonic liquid crystal. The former is an effect long predicted to be possible but never observed for two reasons: first, strong enough magnets were not available, and second, previously known liquid crystal materials have too strong a first-order character to make this observable.

• This work was published in *Physical Review Letters*, **101**, 247801-1-4 (2008).

High Field Magneto-Optical Studies of Liquid Crystals and Complex Fluids

S.N. Sprunt, J.T. Gleeson, A. Jákli, T. Ostapenko, Kent State University

INTRODUCTION

New categories of liquid crystals bring exciting opportunities for both new technological applications and fundamental science. High magnetic fields enable exploration of otherwise inaccessible regions of the phase diagram, and so are an important tool in furthering our understanding of what mesogenic states of matter are possible. Our initial project studied a class of liquid crystals having bent-core or boomerang shape; we have since transitioned into a greater study of biologically compatible materials known as lyotropic chromonic liquid crystals. The key question here, which can only be answered using ultra-high magnetic fields, is whether or not the molecules have formed supermolecular aggregates that are capable of adopting liquid crystalline order.

EXPERIMENTAL

The principal tool for studying liquid crystal material science has always been optics using polarized light. Deploying this tool in Magnet Lab resistive solenoid magnets is a technical challenge. In 2008, during two weeks of magnet time we measured magnetic field induce optical birefringence, optical rotation and circular dichroism in a variety of different liquid crystal formulations. The latter two measurement techniques have not been previously employed on these materials. We were joined by two new collaborators on this project. Dr. Y. Nastishin of the Institute of Physical Optics, Lviv, Ukraine, and Prof. P.J. Collings of Swarthmore College.
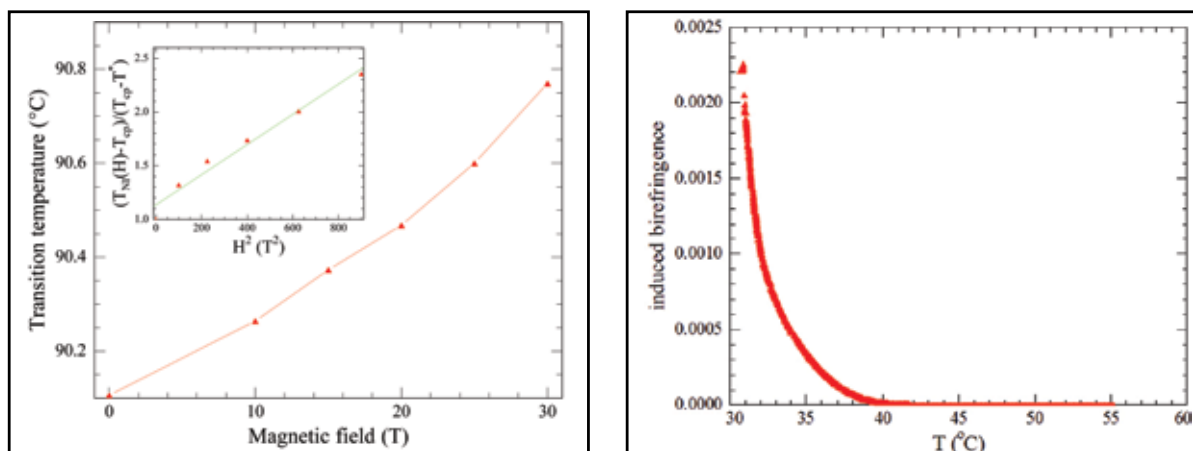
Figure 1.
Left: Liquid crystal transition temperature as function of magnetic field. Inset: Same data plotted in manner predicted by Landau-deGennes theory of nematic isotropic transition. **Right:** Induced birefringence vs. temperature at 25 tesla. At about 8 degrees above the end of the coexistence region, the birefringence becomes abruptly zero.

RESULTS AND DISCUSSION

Our most important results in 2008 were: i) confirmation of a magnetic-field-induced first order phase transition in a bent-core liquid crystal[1], and ii) first-ever observation of the loss of field-induced optical birefringence in a lyotropic chromonic liquid crystal. The former is an effect that has long been known to be possible but had not been previously observed for two reasons: first, strong enough magnets were not available, and second, previously known liquid crystal materials have too strong a first-order character to make this observable.

2008 saw our first investigation into chromonics, and the initial results are tantalizing. Unlike traditional liquid crystals, the structure, which can possess orientational order in chromonics, is a supermolecular aggregate, so in addition to the cooperative effects between aggregates, we must also consider the characteristics of the aggregates themselves. High magnetic field studies at temperatures above where the solution spontaneously exhibits liquid crystalline behavior reveal that at a finite temperature, the birefringence abruptly disappears, indicating the absence of aggregates.

ACKNOWLEDGEMENTS

REFERENCES
1.   T. Ostapenko *et al*., *Physical Review Letters*, **101**, 247801-1—247801-4, (2008).

CONDENSED MATTER PHYSICS

CONDENSED MATTER PHYSICS

> The excitement of the discovery of the pnictide superconductors in 2008 resulted in the Mag Lab hosting several groups competing simultaneously throughout much of the summer. The next three highlights represent some of the most exciting results.

Unlike its As-analog, LaFePO has no high temperature magnetic, spin density wave (SDW) transition and becomes a superconductor at Tc~6 K. Therefore, with their good crystal, the authors were able to observe the "bare" energy spectrum, i.e., Fermi surfaces without the reconstruction caused by the onset of a SDW in most As-pnictides. Remarkably, the resulting spectrum reproduces in all details the main features of Fermi surfaces obtained in numeric calculations: the quasi- two-dimensionality and the pronounced nesting character. Note that all pnictides seem to be rather similar as far as their "bare" electronic properties are concerned.

Fermi Surface of Superconducting LaFePO Determined from Quantum Oscillations

A.I. Coldea, J. D. Fletcher, A. Carrington, A. F. Bangura, N. E. Hussey (Bristol University, UK); J. G. Analytis, J.-H. Chu, A. S. Erickson, I. R. Fisher (Stanford University); R. D. McDonald (Magnet Lab-LANL)

LaFePO is a newly discovered bulk Fe-based superconductor with a transition temperature of $Tc \sim 6$ K[1]. This compound is isostructural with LaFeAsO, which is non-superconducting and has a spin-density wave (SDW) ground state at low temperatures; when electron doped it becomes a relatively high-Tc superconductor ($Tc \sim 25$ K)[2]. Understanding the superconductivity in Fe-based superconductors is intimately related to the details of the Fermi surface topology, its tendency towards instabilities as well as the strength of the coupling of the quasiparticles to excitations. Among pairing mechanisms mediating the superconductivity magnetic fluctuations are a possible candidate due to the proximity of the superconducting state to magnetic antiferromagnetic phase, as in cuprates but in fero-oxypcnities the nesting of the Fermi surface could be responsible for stabilizing the magnetic state. LaFePO is an ideal test material to investigate the Fermi surface topology as it has a much lower Tc among the other structurally related pcnitites, is non-magnetic and does not suffer any structural transitions at low temperatures. Moreover, its normal state can be easily accessed in moderate magnetic fields and high quality single crystalline materials can be grown.
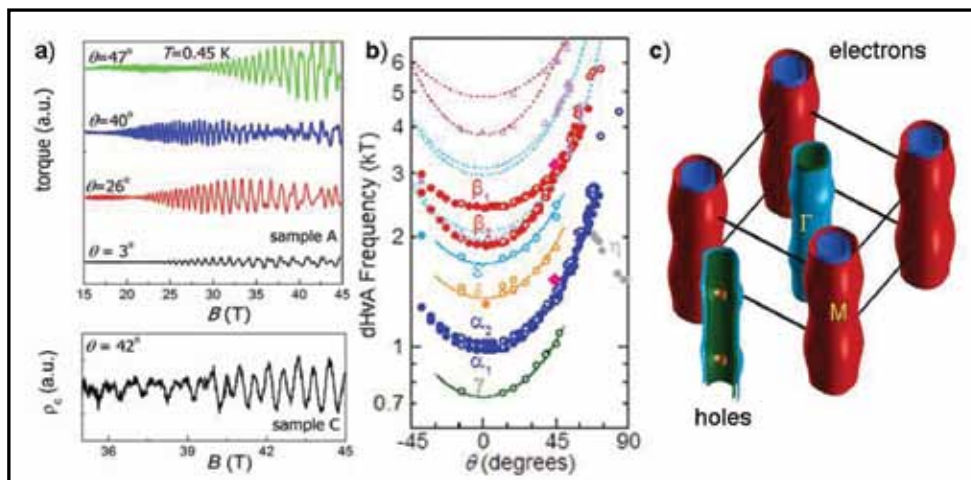

Figure 1. Quantum oscillations in the superconducting LaFePO. a) The oscillatory part of torque and interplane transport as function of magnetic field for different orientations between magnetic field and the *c* axis. b) The angular dependence of the fundamental frequencies (related to the extremal areas of the Fermi surface). The resulting Fermi surface of LaFePO.

We have recently observed quantum oscillations in LaFePO using the Hybrid magnet in Tallahassee up to 45 tesla (T) and at low temperatures 0.5 K[3]. By using both a thermodynamic – torque using piezoresistive microcantilevers (sample A) – and transport (sample C) techniques down to 0.3 K, we have been able to map

the angular dependence of the Fermi surface extremal areas and also the elect of electronic correlations in LaFePO (Figure 1a). While four main frequencies (β_1 and β_2 closely split frequencies at $F\sim1kT$) and the two higher frequencies (β_1 and β_2) are observed clearly up to 18 T, only extending the field range to 45 T in Tallahassee we were able to identify the orbits with smaller amplitudes (γ, δ, ε) (Figure 1b). Our results are in broad agreement with the band-structure calculations with the quasiparticle mass enhanced by a factor 2. Our observation suggests that the quasi-two dimensional Fermi surfaces of LaFePO consist of nearly-nested electron and hole pockets, suggesting proximity to a spin/charge density wave instability[3].

REFERENCES
1. Y. Kamihara *et al.*, *J. Am. Chem. Soc.*, **128**, 10012 (2006).
2. Y. Kamihara *et al.*, *J. Am. Chem. Soc.*, **130**, 3296 (2008)
3. Coldea, A.I., *et al.*, *Phys. Rev. Lett*, **101**, 216402 (2008).

Magnetic/structural transition in $SrFe_2As_2$ with the vector Q= (1/2, 1/2, 0) is expected to reconstruct the "bare" Fermi surface (FS). Contactless resistance measurements performed on the 60 tesla long-pulse magnet at Los Alamos reveal that only tiny pockets may survive the onset of such a spin density wave. Carriers in these small pockets still guarantee good metallic behavior. The results are in favor of the inter-band nesting origin of SDW. It remains unclear whether these results agree well with angle resolved photoemission spectroscopy.

• This work was published in the *Journal of Physics-Condensed Matter*, **20** (42), 422203 (2008).

Quantum Oscillations in the Parent Phase of an Iron Arsenide Superconductor

Suchitra E. Sebastian, J. Gillett (Cambridge University); N. Harrison, C. H. Mielke (Magnet Lab-LANL); G. G. Lonzarich (Cambridge University)

We utlized the 60 T long-pulse magnet at the Magnet Lab, Los Alamos to observe quantum oscillations for the first time on the parent magnetic phase of a high temperature superconductor $SrFe_2As_2$, revealing a Fermi surface comprising tiny pockets of carriers. A Fermi surface reconstructed by $Q = (\pi,\pi,0)$ for itinerant antiferromagnetic ordering (indicated by inelastic neutron scattering experiments) in $SrFe_2As_2$ is expected to
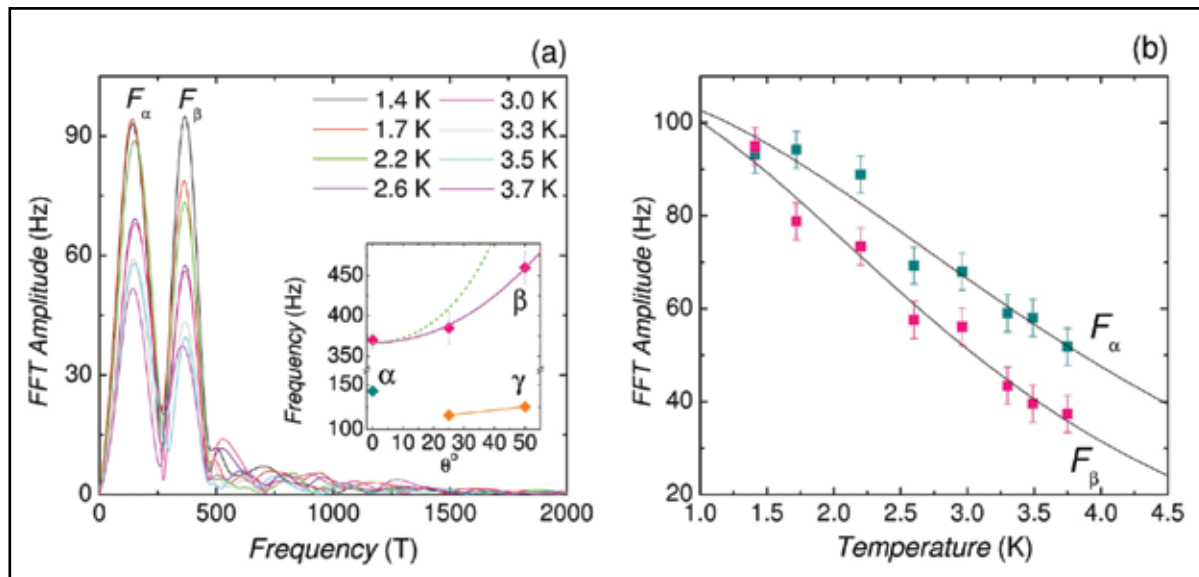

Figure 1.
a) The tunnel diode oscillator (TDO) resonance frequency measured as a function of magnetic field;
b) Quantum oscillations in the TDO frequency obtained on performing a background polynomial subtraction are shown at a series of different temperatures

CONDENSED MATTER PHYSICS

yield small pockets of varying size, in agreement with the quantum oscillations observed in our experiments. Our present results indicate that strong correlations in the parent antiferromagnetic phase of pnictide superconductors are no obstacle to the establishment of conventional metallic behavior.
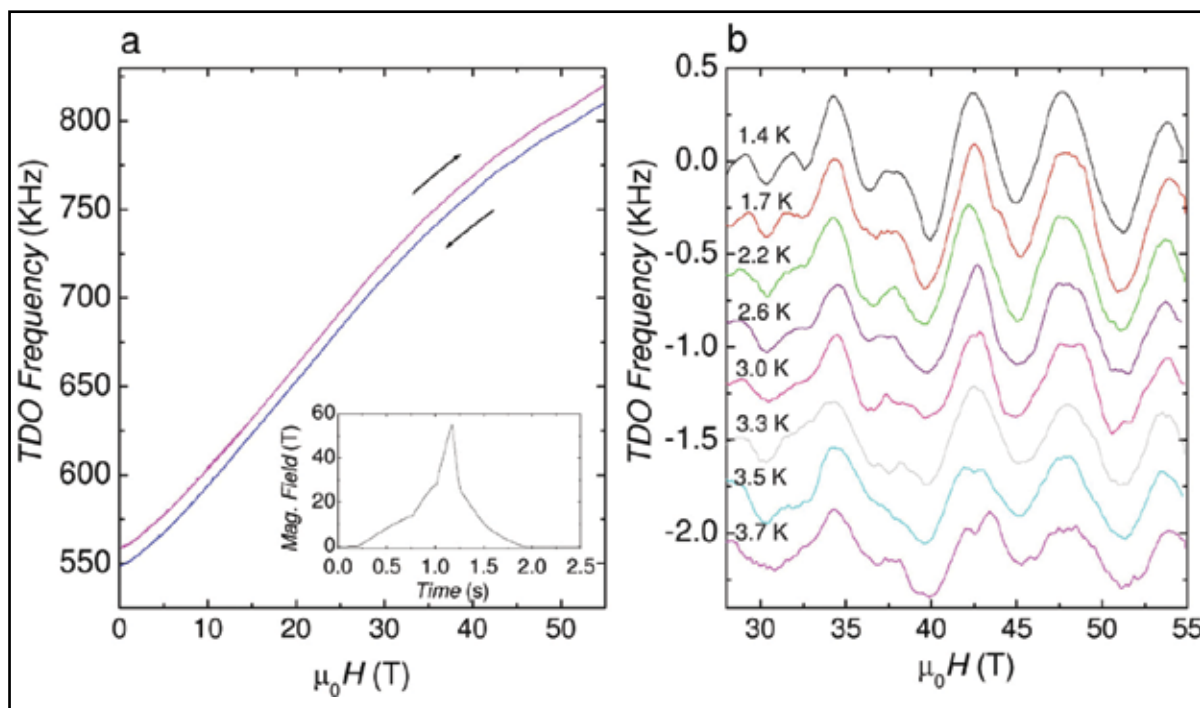

Figure 2.
a) Fourier transform of the quantum oscillations performed.
b) A fit of the experimental temperature-dependent amplitudes to the Lifshitz-Kosevich thermal damping term.

REFERENCE

"Quantum oscillations in the parent magnetic phase of an iron arsenide high temperature superconductor," Suchitra E. Sebastian et al., J. Phys.: Condens. Matter, **20** No 42 422203 (2008).

On single crystals of (Ba,K,)Fe$_2$As$_2$ it was shown that anisotropy of the critical fields is small enough and one may consider these superconductors three-dimensional.

• This work was published in Nature, **457** (7229), 565-568 (2009).

Nearly Isotropic Superconductivity in (Ba,K)Fe$_2$As$_2$

H. Q. Yuan (Physics, Zhejiang University; Magnet Lab-LANL); J. Singleton, F. F. Balakirev, S. Baily (Magnet Lab-LANL); G. F. Chen, J. L. Luo, N. L. Wang (Chinese Academy of Science)

INTRODUCTION

Furious scientific activity has been generated by the recent discovery of superconductivity in the iron-arsenic-based compounds ReFeAs(O,F) (Re = lanthanide) and (A,K)Fe$_2$As$_2$ (A=Ba, Sr)[1]. Superconducting transition temperatures T_c as high as 55 K have been observed, naturally provoking comparisons with the well-known "high T_c" cuprate superconductors. The layered crystal structure of the cuprates (which leads to quasi-two-dimensional electronic properties) led to speculations that reduced dimensionality is a necessary prerequisite for superconductivity at temperatures above 40 K; at first sight, the iron-arsenic compounds, which also possess layered structures, give additional credence to this idea. However, our measurements in magnetic fields of up to 60 tesla (T), necessary to overcome the large upper critical fields, demonstrate that the superconducting properties of single crystals of (Ba,K)Fe$_2$As$_2$ are in fact rather three dimensional[1]. This is markedly different from the highly anisotropic properties of all previously known layered superconductors (e.g. the cuprates and the crystalline organic metals); we suggest that it is attributable to the distinctive Fermi surfaces of the iron-arsenide compounds.

EXPERIMENTAL

The magnetoresistance of high-quality, single-crystal samples was measured using the Mag Lab's digital lockin technology. The 50, 60 and 65 T short-pulse magnets at Los Alamos Pulsed Field Facility were employed for the experiments.

RESULTS AND DISCUSSION

Figure 1 shows that the upper critical field of $(Ba,K)Fe_2As_2$ is rather isotropic. As far as we are aware, no other layered superconductors exhibit upper critical fields that behave in this way. The difference is, we believe, associated with $(Ba,K)Fe_2As_2$'s distinctive Fermi-surface topology, the strong corrugations of which – a manifestation of essentially three-dimensional bandstructure – permit orbital limiting of the upper critical field at all field orientations. Therefore the 112-type ternary iron arsenides are unique in possessing both a rather high critical temperature and essentially three-dimensional electronic properties. In contrast to common assumptions based on the properties of the cuprates, it seems that reduced dimensionality is not necessarily a prerequisite for "high-temperature" superconductivity.
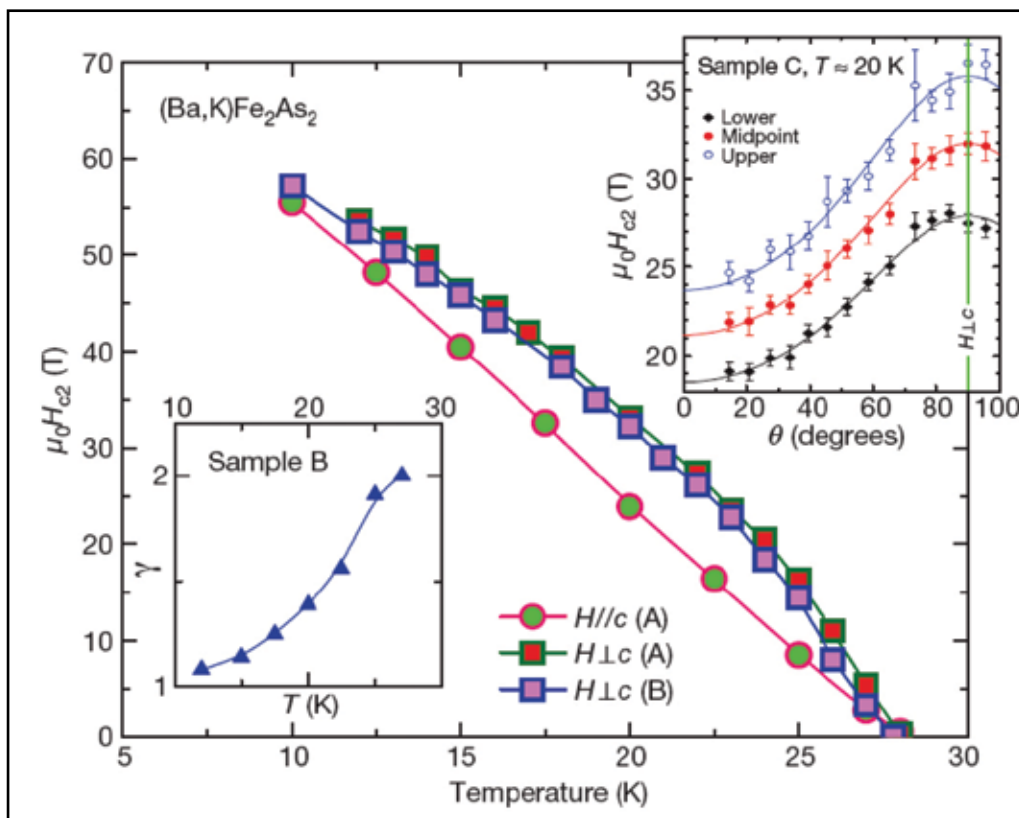

Figure 1.

The upper critical field $H_{c2}(T)$ of $(Ba,K)Fe_2As_2$. The main figure shows H_{c2} versus temperature T for magnetic fields parallel to the c-axis (circles) and perpendicular to the c-axis (squares); in each case $H_{c2}(T)$ values are determined from the midpoint of the sharp resistive superconducting transitions. The two single-crystal samples (A and B) behave nearly identically.

Inset a: The anisotropy parameter γ plotted as a function of temperature; it is about 2 near T_c, a value close to that derived by other groups using low-field measurements, but approaches 1 as $T \rightarrow 0$, indicating isotropic superconductivity.

Inset b: The upper critical field derived at the upper, midpoint and lower limits of the main resistive transition, versus the angle between the applied magnetic field (H) and the crystallographic c axis ($T = 20.3$ K).

ACKNOWLEDGEMENTS

REFERENCES

1. H.-Q Yuan *et al.*, *Nature*, **457** (7229), 565-568 (2009).